Available online at www.sciencedirect.com
SCIENCE DIRECT®
Geochimica et Cosmochimica Acta 70 (2006) 1581–1600
Geochimica
www.elsevier.com/locate/gca

Comparative petrology, geochemistry, and petrogenesis of evolved, low-Ti lunar mare basalt meteorites from the LaPaz Icefield, Antarctica

James M.D. Day [a,*], Lawrence A. Taylor [a], Christine Floss [b], Allan D. Patchen [a], Darren W. Schnare [a], D. Graham Pearson [c]

[a] *Planetary Geosciences Institute, Department of Earth and Planetary Sciences, University of Tennessee, Knoxville, TN 37996, USA*
[b] *Laboratory for Space Sciences, Washington University, St. Louis, MO 63130, USA*
[c] *Arthur Holmes Isotope Geology Laboratory, Department of Earth Sciences, University of Durham, Science Laboratories, South Road, Durham, DH1 3LE, UK*

Received 6 May 2005; accepted in revised form 15 November 2005

Abstract

New data is presented for five evolved, low-Ti lunar mare basalt meteorites from the LaPaz Icefield, Antarctica, LAP 02205, LAP 02224, LAP 02226, LAP 02436, and LAP 03632. These basalts have nearly identical mineralogies, textures, and geochemical compositions, and are therefore considered to be paired. The LaPaz basalts contain olivine (Fo_{64-2}) and pyroxene ($Fs_{32}Wo_8En_{60}$ to $Fs_{84-86}Wo_{15}En_{2-0}$) crystals that record extreme chemical fractionation to Fe-enrichment at the rims, and evidence for silicate liquid immiscibility and incompatible element enrichment in the mesostasis. The basalts also contain FeNi metals with unusually high Co and Ni contents, similar to some Apollo 12 basalts, and a single-phase network of melt veins and fusion crusts. The fusion crust has similar chemical characteristics to the whole rock for the LaPaz basalts, whereas the melt veins represent localized melting of the basalt and have an endogenous origin. The crystallization conditions and evolved nature of the LaPaz basalts are consistent with fractionation of olivine and chromite from a parental liquid similar in composition to some olivine-phyric Apollo 12 and Apollo 15 basalts or lunar low-Ti pyroclastic glasses. However, the young reported ages for the LaPaz mare basalts (~2.9 Ga) and their relative incompatible element enrichment compared to Apollo mare basalts and pyroclastic glasses indicate they cannot be directly related. Instead, the LaPaz mare basalts may represent fractionated melts from a magmatic system fed by similar degrees of partial melting of a mantle source similar to that of the low-Ti Apollo mare basalts or pyroclastic glasses, but which possessed greater incompatible element enrichment. Despite textural differences, the LaPaz basalts and mare basalt meteorite NWA 032 have similar ages and compositions and may originate from the same magmatic system on the Moon.

1. Introduction

Apollo and Luna sample collection missions to the Moon arguably represented the zenith of space exploration in the 20th century. Subsequent to these missions, additional lunar samples have been provided through the discovery and on-going collection of meteorites from the Antarctic and hot desert regions. So far, attempting to provenance lunar meteorites to their source locations on the Moon has been challenging, but some probably originate from regions of the Moon not sampled during the Apollo or Luna missions. Of the lunar meteorites, only a few are mare basalts, with a much larger proportion representing basaltic, mingled or anorthositic regolith breccias. Nevertheless, the mare basalt meteorites have proffered new insight into lunar petrogenesis and the evolution of the Moon's mantle (e.g., Borg et al., 2004; Gnos et al., 2004; Korotev, 2004). It is notable that of the mare basalt meteorites discovered to date, all can be classified as low-Ti or very-low-Ti (VLT), with the majority being relatively evolved when compared with low-Ti Apollo 12 and Apollo 15 mare basalt suites.

* Corresponding author.
E-mail address: jday13@utk.edu (J.M.D. Day).

0016-7037/$ - see front matter © 2005 Elsevier Inc. All rights reserved.
doi:10.1016/j.gca.2005.11.015

Here, we investigate the mineralogical and geochemical attributes of the LaPaz mare basalt meteorites. Collectively paired, LaPaz mare basalt meteorites make only the sixth unbrecciated lunar mare basalt found on Earth after Yamato-793169, Asuka-881757, NWA 032/479, and clasts from breccias Dhofar 287 and NWA 773.

Lunar mare basalt meteorites LAP 02205 (1226.3 g), LAP 02224 (252.5 g), LAP 02226 (244.1 g), LAP 02436 (59.0 g), and LAP 03632 (92.6 g) were discovered in the LaPaz Icefield, Antarctica during the 2002/2003 ANSMET field season. Combined, these meteorites represent the largest suite of mare basalts found in a single locale on Earth (1.88 kg). In this contribution, we show that the LaPaz mare basalts represent a significant mass of young (~2.9 Ga), evolved, incompatible element enriched lunar lavas unlike any samples available in the Apollo or Luna collections. Furthermore, these basalts appear to originate from the same source as NWA 032 on the Moon.

2. Analytical methods

Eleven polished thin sections (LAP 02205, 36 and 42; LAP 02224, 26 and 28; LAP 02226, 19 and 20; LAP 02436, 18 and 26, and LAP 03632, 6, 21 and 24; surface areas range from 50 to 150 mm^2) of the LaPaz meteorites were obtained from the meteorite working group (MWG) for petrographic and mineralogical examination. Mineral modes were determined on eight polished sections with the *Feature Scan Phase Distribution* software package of an Oxford instrument energy dispersive spectrometer (EDS) interfaced to the CAMECA SX-50 electron microprobe analyzer (EMPA) at the University of Tennessee. Modal analysis acquisition was performed using an accelerating potential of 15 keV, a 4 nA beam current and 70 mS count times sampling every 8 μm (Taylor et al., 1996). Data bin parameters for this method are provided in Table 1 and run conditions for modal analysis were identical for all polished sections.

Mineral compositions were determined in wavelength dispersive spectral (WDS) mode on the EMPA using an accelerating potential of 15 keV, a 20 nA beam current (30 nA for metals), 1 μm beam size, peak and background counting times of 20–30 s and standard ZAF (PAP) correction procedures. Glass and plagioclase compositions were determined using a 10 nA beam current a 5–10 μm beam size and longer counting times to avoid mobilization of Na. A combination of natural and synthetic standards were used for calibration and were measured periodically within analytical sessions to ensure data quality. Drift was within counting error throughout every analytical session. Detection limits (3σ above background) are typically <0.03 for SiO_2, TiO_2, Al_2O_3, MgO, CaO, Na_2O, K_2O, and Cl, <0.05 for Cr_2O_3, MnO, FeO, P_2O_5 NiO, and Co, and <0.05–0.1 for all other oxides and elements listed.

Concentrations of trace elements, including REE, were determined using the modified Cameca ims 3f ion micro-

Table 1
Modal analysis of LaPaz mare basalt meteorites and comparison with other mare basalt modal percentages

	LAP 02205, 31	LAP 02205, 42	LAP 02224, 26	LAP 02224, 28	LAP 02226, 19	LAP 02226, 20	LAP 02436, 18	LAP 02632, 06	Average	SD	%RSD	Dhofar 287A[a]	NWA 032[a]	Y-793169[a]	A-881757[a]	12016[a]	12054[a]	15556[a]
Volume %																		
Clinopyroxene	44.0	43.4	43.6	41.3	44.1	41.7	42.9	42.4	42.9	1.0	2.4	18.1	—	—	—	—	—	—
Plagioclase	33.7	34.8	32.2	33.3	32.1	35.4	32.8	32.8	33.4	1.2	3.6	25.9	29.4	42.0	30.0	29.1	27.9	38.0
Pigeonite	11.5	11.7	12.41	11.1	11.7	11.3	11.7	12.4	11.7	0.4	3.6	29.3	—	—	—	—	—	—
Ilmenite	3.3	3.5	3.0	3.7	3.5	3.2	3.3	3.5	3.4	0.2	6.4	2.3	4.4	1.0	6.0	4.8	5.2	2.1
Melt (Vein, Fusion)	1.5	1.9	2.1	1.3	1.9	1.6	2.1	1.2	1.7	0.4	21.0	1.4	3.2	<0.1	<0.1	<0.1	<0.1	<0.1
Fayalite	1.4	1.41	1.5	2.2	1.6	1.9	2.0	1.9	1.7	0.3	20.3	0.2	—	—	—	—	—	—
Olivine	1.2	0.5	1.9	3.1	1.3	1.7	1.6	1.9	1.6	0.8	45.7	20.5	11.3	<0.1	<0.1	12.0	10.8	<0.1
K-Glass	0.7	0.6	0.7	0.8	0.6	0.6	0.8	0.7	0.7	0.1	11.5	<0.1	<0.1	<0.1	<0.1	0.6	1.9	1.0
Troilite	0.2	0.2	0.2	0.2	0.2	0.2	0.2	0.2	0.2	0.02	7.7	0.1	0.7	<0.1	—	<0.1	0.3	<0.1
Ulvöspinel	0.4	0.3	0.5	0.3	0.4	0.3	0.4	0.3	0.4	0.1	16.6	0.8	—	<0.1	—	<0.1	0.5	0.6
Chromite	0.1	0.1	0.2	0.2	0.1	0.1	0.1	0.2	0.1	0.05	42.2	0.4	0.3	<0.1	—	<0.1	1.9	0.4
Phosphate	0.3	0.3	0.2	0.3	0.2	0.3	0.2	0.2	0.2	0.03	12.1	0.6	—	—	—	—	—	—
FeNi metal	<0.1	<0.1	<0.1	<0.1	<0.1	<0.1	<0.1	<0.1	<0.1	—	—	<0.1	—	—	—	—	<0.1	—

Modal percentage data from this study or from [a]Anand et al. (2003).
Data bins defined according to: Clinopyroxene = 47–72% Si, 11–41.5% Ca, 7–42% Fe; Pigeonite = 46–72% Si, 4–12% Ca, 10–46% Fe; Plagioclase = 20–46% Al, 35–55% Si, 15–40% Al; Ilmenite = 45–74% Ti, 15–43% Fe; Fayalite = 20–42% Si, 0–4% Ca, 45–75% Fe; Olivine = 10–45% Mg, 30–53% Si; Ulvöspinel = 20–45% Ti, 0–28% Cr; Cr-Spinel = 20–74% Cr, 0–20% Ti; Melt = 8–12% Al, 39–60% Si, 9–20% Ca; K-Glass = 55–100% Si, 6–22% Al, 3–25% K (other classifications obtainable from the corresponding author upon request).

probe at Washington University, according to techniques described by Zinner and Crozaz (1986a). All analyses were made using an O^- primary beam and energy filtering at low mass resolution to remove complex molecular interferences. The resulting mass spectrum is deconvolved in the mass ranges K–Ca–Sc–Ti, Rb–Sr–Y–Zr and Ba–REE to remove simple molecular interferences that are not eliminated with energy filtering (Alexander, 1994; Hsu, 1995). Sensitivity factors for the REE are from Zinner and Crozaz (1986b) and those for other elements are from Hsu (1995) and are listed in Table 1 of Floss et al. (1998). Absolute concentrations were determined using sensitivity factors relative to Si for silicates and Ca for phosphates, with SiO_2 and CaO concentrations determined by EMPA of the specific grains chosen for ion probe analysis. Reported errors are 1σ and are due to counting statistics only.

1.5–2.0 g of each sample was provided by the MWG for whole rock geochemical studies (LAP 02205, 21; LAP 02224, 17 & 18; LAP 02226, 13; LAP 02436, 20 and LAP 03632, 08). The entire allocated mass of each sample was crushed and homogenized using an agate pestle and mortar under better than class 100 air flow. Whole rock powder aliquots (~10 mg) were fused into glass beads on a Mo-strip resistance heater, in a nitrogen atmosphere. Fused bead major element concentrations were analyzed using the EMPA and protocols for glass analyses. The average of 15 spot analyses are reported on a Mo-free basis (Measured $Mo_2O = 0.46 \pm 0.22$ wt%). Trace element concentrations were measured on unfused 20 mg aliquots using an ELAN 6000 Inductively Coupled Plasma-Mass Spectrometer at the University of Durham following the procedure of Ottley et al. (2003). The remaining unfused sample mass is being used for on-going isotopic studies of these meteorites (e.g., Day et al., 2005a).

3. Results

3.1. Petrography and textures

The LaPaz meteorites have nearly identical textures (Fig. 1) for their constituent mineralogies. They are holocrystalline, intergranular to subophitic basalts predominantly composed of pigeonite, augite, ferropyroxene, plagioclase, and ilmenite (Table 1; Fig. 1), with accessory phases of silica (tridymite/cristobalite), olivine, ulvöspinel, chromite, phosphates, troilite, and FeNi metal grains. Mesostasis areas represent up to 3% of the polished sections studied and are composed of glass and fayalite with minor baddeleyite, fluorapatite, merrillite, barium K-feldspar, and a rare zirconium- and titanium-rich mineral, that stoichiometrically is zirkelite ($(Ca,Th,Ce)Zr(Ti,Fe^{2+},Nb)_2O_7$). In addition to these phases, shock-induced melt veins and, in three polished sections studied, fusion crusts also occur.

Data for modal analyses of LaPaz basalts and other low-Ti mare basalt meteorites are presented in Table 1. The LaPaz mare basalts have identical mineralogies and nearly identical modal abundances of main mineral phases. Percentage relative standard deviations are low for the main mineral phases, clinopyroxene (RSD% = 2.4), pigeonite (RSD% = 3.6), and plagioclase (RSD% = 3.6), but are greater and more variable for accessory minerals. Compared with other mare basalt meteorites, LaPaz basalts have lower abundances of forsteritic olivine than Dhofar 287A (the large unbrecciated basalt clast of Dhofar 287; Anand et al., 2003), NWA 773 or NWA 032 and lower abundances of plagioclase than Y-793169 or A-881757.

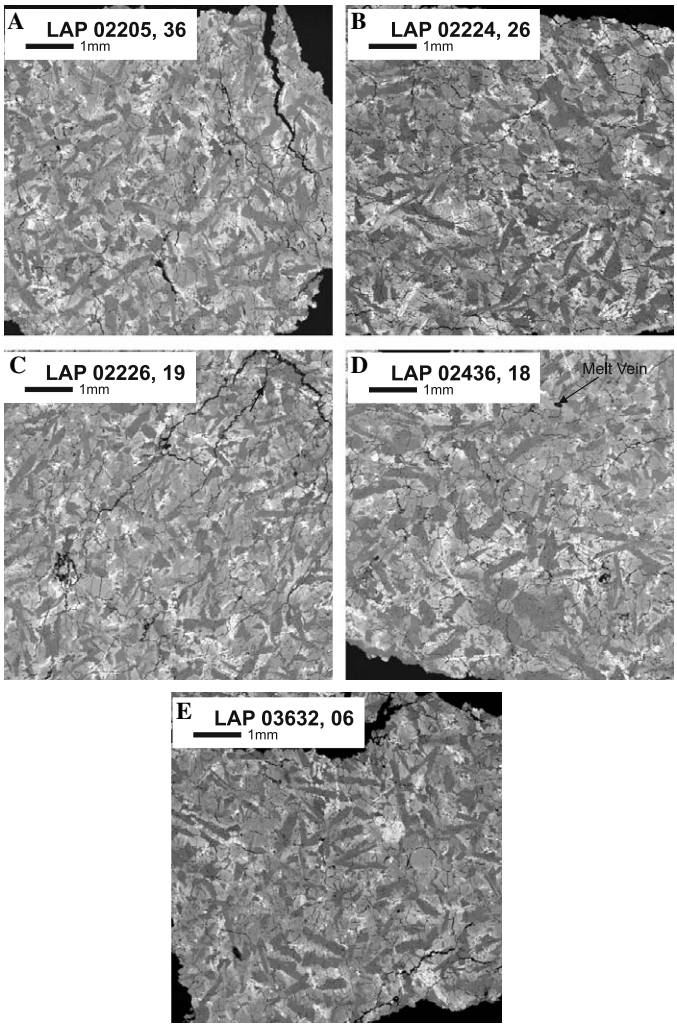

Fig. 1. Back-scattered electron images of the LaPaz basalts. Note the nearly identical textures and mineralogies. The darkest phases are plagioclase (elongate) and silica, brightest phases are ilmenite (elongate), fayalite, and spinels. Intermediate grayscales represent pyroxene, forsteritic olivine, and melt veins (indicated). (A) LAP 02205, 36; (B) LAP 02224, 26; (C) LAP 02226, 19; (D) LAP 02436, 18; (E) LAP 03632, 06.

The LaPaz basalts all contain abundant petrographic evidence for impact-induced shock effects, possibly related to the ejection event that launched them from the lunar surface. Shock effect features include a dentritic, single-phase collection of zoned, banded, sinuous melt veins and melt pockets, often with single large vesicles, undulatory extinction to partial maskelynitization of plagioclase, mosaic fracture and planar deformation of pyroxene and olivine,

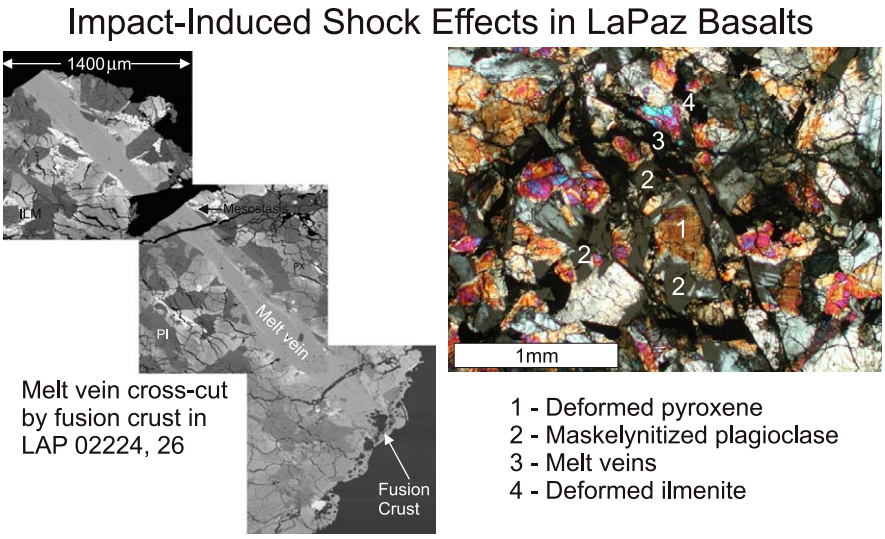

Fig. 2. Impact-induced shock features of the LaPaz basalts showing a composite back-scattered electron image of a large melt vein cross-cut by fusion crust. Note the zonation of the melt vein and the frothy texture of the fusion crust. ILM, ilmenite; Pl, plagioclase; PX, pyroxene. Also shown is a transmitted light photomicrograph of a portion of LAP 02436 showing (1) crystal-deformed pyroxene, (2) maskelynitized to partially maskelynitized plagioclase, (3) a single-phase network of melt veins, and (4) crystal-deformed ilmenite. These shock features occur in all of the LaPaz mare basalt meteorites.

and step-like fractures in ilmenite (Fig. 2). These features indicate heterogeneous shock in the range of <30 to >75 GPa (e.g., Kieffer et al., 1976). The LaPaz mare basalt meteorites were discovered on the ice with a ~50–95% coating of vitric fusion crust with flow lines and regmaglypts (McBride et al., 2004). Such features are common to lithic materials that have passed through the Earth's atmosphere at high velocity.

3.2. Mineral chemistry

The following section describes the petrography and chemical compositions of minerals in order of their relative modal abundance.

3.2.1. Pyroxene (Modal abundance-55%)

Pyroxene is the most abundant mineral in the LaPaz basalts (Table 1) and occurs as equant, intersertal crystals (average length and width = 0.28 × 0.17 mm) that sometimes possess shock-related lamellae. EMPA traverses show that these features are not exsolution lamellae (i.e., related to cooling rate). Pyroxene compositions range from pigeonite (Wo_8En_{60}) to ferroaugite, ferropigeonite and extreme Fe-enrichment to pyroxferroite ($Fs_{84–86}Wo_{15}En_{2–0}$; Table 2; Fig. 3). Pigeonite cores possess Ti/Al (atomic) ratios <0.5 and Ti/(Ti + Cr) (atomic) ratios 0.4–0.6. With crystallization, a steady decrease in Mg/(Mg + Fe) to ferroaugite compositions results in a sharp change in Ti/Al ratios to >0.5 with significantly lower Al concentrations and increase in Ti/(Ti + Cr), all the way to Fe-pyroxene compositions (Fig. 4). This change in Al, Cr, and Ti pyroxene crystal chemistry with Mg/(Mg + Fe) has previously been interpreted as reflecting pigeonite crystallization followed by near-simultaneous crystallization of augite, plagioclase and ilmenite in Apollo 12 and 15 basalts (e.g., Bence and Papike, 1972).

Representative SIMS data for minerals from LAP 02224 and LAP 02205 are presented in Table 3. Pyroxene rare earth element (REE) profiles for LAP 02205, 36 and LAP 02224, 26 have convex upward, sub-parallel patterns, large negative Eu anomalies and increasing REE abundances with greater Fe-enrichment (Fig. 5). Some pyroxenes in the LaPaz basalts show flat or slightly REE-enriched patterns similar to those found in brecciated mare basalt meteorite NWA 773 (Jolliff et al., 2003). In polished sections that possess fusion crust, and hence are near the exposed surface of their respective meteorites, the pyroxenes possess Ce-anomalies (e.g., LAP 02224, 26) due to terrestrial weathering, whereas further from the surface and in the larger mass meteorites, they do not (e.g., LAP 02205, 36; Anand et al., 2005). Previously, it has been demonstrated that the terrestrial alteration systematics of Antarctic Meteorites can be quite variable and that the degree of alteration probably relates to fracturing in silicate grains (Floss and Crozaz, 1991; Crozaz et al., 2003).

3.2.2. Plagioclase (33%)

Plagioclase in the LaPaz basalts occurs as tabular crystals (average length and width = 0.27 × 0.10 mm) that are only partially converted to maskelynite. Plagioclase compositions ($An_{79–93}$) are relatively typical of the fractionation trend for low-Ti Apollo 12 and Apollo 15 mare basalts (Table 2; Fig. 6). Plagioclase grains generally possess between 23 and 47 ppm Ba, 180–240 ppm Sr, ⩽0.2 wt% MgO and K_2O, and ⩽0.8 wt% FeO. Plagioclase crystals have relatively flat REE patterns with positive Eu anomalies and lower REE abundances at high An contents (Fig. 5). Cooling-rate estimates based upon plagioclase lath

Table 2
Representative EMPA data for main silicate minerals, phosphates and accessory phases in the LaPaz mare basalt meteorites

Phases:	Pyroxene					Fe-Px		Olivine				
Sample:	LAP 02205	LAP 02224	LAP 02226	LAP 02436	LAP 03632	LAP 03632	LAP 02436	LAP 02205	LAP 02224	LAP 02226	LAP 02436	LAP 03632
wt%												
SiO_2	51.4	51.2	50.9	50.7	51.3	45.0	44.4	36.2	36.0	36.4	36.4	36.5
TiO_2	0.66	0.70	0.64	0.68	0.68	1.85	1.70	0.03	—	—	0.04	0.06
Al_2O_3	1.36	1.12	1.66	1.63	1.54	1.20	1.58	0.04	—	—	⩽0.03	0.04
Cr_2O_3	0.56	0.47	0.74	0.71	0.72	⩽0.05	⩽0.05	0.15	0.24	0.63	0.19	0.29
MgO	16.3	16.5	19.0	19.4	18.7	1.00	0.32	30.6	31.3	31.2	31.3	31.9
CaO	13.2	8.63	8.04	6.1	7.82	8.64	16.8	0.37	0.37	0.29	0.31	0.35
MnO	0.31	0.31	0.32	0.38	0.32	0.50	0.40	0.36	0.36	0.34	0.33	0.28
FeO	15.9	21.0	18.3	19.5	17.9	41.4	33.8	32.8	31.4	30.3	31.7	30.0
Na_2O	0.05	⩽0.03	⩽0.03	⩽0.03	⩽0.03	⩽0.03	⩽0.03	—	—	—	—	—
NiO	—	⩽0.03	—	—	—	—	—	—	—	—	—	—
Total	99.6	100.0	99.6	99.1	99.0	99.6	99.0	100.6	99.7	99.1	100.3	99.4
Mg#	65	58	65	64	65	4	1.6	62	64	65	64	52

Phases:	Fayalite		Plagioclase		Ba-rich plag	Si-glass	K-Ba-glass	Apatite		Merrillite		Baddelyite
Sample:	LAP 02205	LAP 02436	LAP 02205	LAP 02436	LAP 03632	LAP 03632	LAP02224	LAP 03632	LAP 03632	LAP 02436	LAP 03632	LAP 03632
wt%												
SiO_2	28.9	29.4	47.1	46.5	52.5	98.4	75.0	1.66	1.32	0.33	0.45	2.23
TiO_2	0.15	0.16	—	—	0.12	0.20	0.67	—	—	—	—	5.03
ZrO_2	—	—	—	—	—	—	—	—	—	—	—	80.8
Al_2O_3	0.04	⩽0.03	32.8	32.7	21.0	0.37	10.9	0.06	0.05	0.06	0.04	0.14
Cr_2O_3	⩽0.05	⩽0.05	—	—	—	—	⩽0.05	—	—	—	—	—
MgO	0.46	0.22	0.23	0.25	⩽0.03	⩽0.03	⩽0.03	⩽0.03	⩽0.03	0.13	0.21	⩽0.03
CaO	0.65	0.70	17.6	17.8	0.58	0.05	1.68	52.3	53.0	40.4	40.0	1.71
MnO	0.69	0.74	—	—	⩽0.03	⩽0.03	⩽0.03	—	—	—	—	⩽0.03
FeO	68.4	67.9	0.72	0.58	0.81	0.55	2.91	2.20	1.32	7.39	6.29	3.52
P_2O_5	—	—	—	—	⩽0.03	⩽0.03	—	39.6	40.3	42.1	42.7	—
BaO	—	—	—	—	14.2	⩽0.03	1.04	—	—	—	—	—
Na_2O	—	—	1.24	1.14	0.23	⩽0.03	0.17	⩽0.03	⩽0.03	0.09	0.23	—
K_2O	—	—	⩽0.03	0.05	10.0	⩽0.03	6.98	⩽0.03	⩽0.03	0.04	⩽0.03	—
Y_2O_3	—	—	—	—	—	—	—	—	—	—	—	1.42
Nb_2O_3	—	—	—	—	—	—	—	—	—	—	—	1.54
La_2O_3	—	—	—	—	—	—	—	0.18	0.19	0.73	0.79	0.09
Ce_2O_3	—	—	—	—	—	—	—	0.46	0.58	2.01	2.21	0.17
SO_2	—	—	—	—	—	—	—	0.30	0.11	0.05	⩽0.05	—
F	—	—	—	—	—	—	—	1.38	2.68	0.18	0.34	—
Cl	—	—	—	—	—	—	—	0.71	0.24	⩽0.03	⩽0.03	—
O = (F, Cl)	—	—	—	—	—	—	—	−0.74	−1.18	—	—	—
Total	99.3	99.2	99.7	99.1	99.4	99.6	99.4	98.0	98.6	93.5	93.3	96.7
Mg#	1.2	0.6										

Fe-Px = Evolved Fe-rich pyroxene.

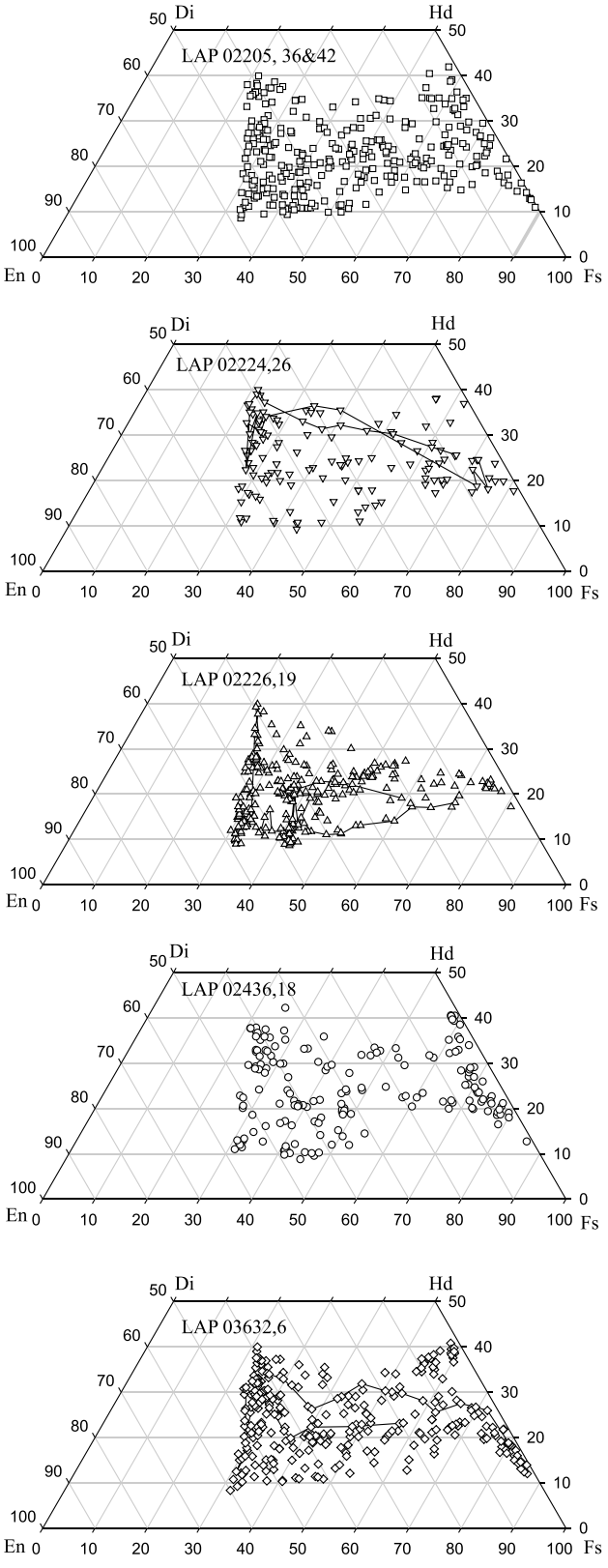

Fig. 3. Enstatite-Diopside-Hedenbergite-Ferrosilite pyroxene quadrilaterals for LaPaz basalts LAP 02205, LAP 02224, LAP 02226, LAP 02436, and LAP 03632. Plots show the extreme zonation of pyroxenes from low Ca, high Mg cores to rim compositions that approach ferrohedenbergite or pyroxferroite. Lines indicate measured EMPA traverses across single pyroxene grains.

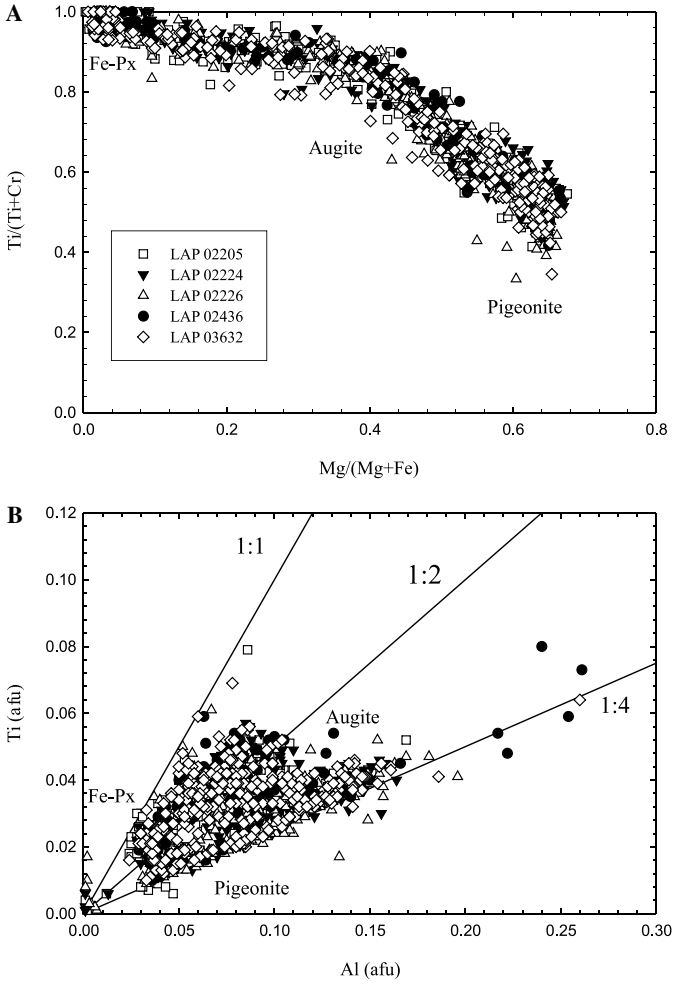

Fig. 4. Plots of (A) Ti/(Ti + Cr) versus Mg/(Mg + Fe) and (B) Ti versus Al (atomic formula units) for LaPaz pyroxenes after Bence and Papike (1972). Pyroxene compositions range from high Mg-number, low Ti-number pigeonites to low Mg-number ferropyroxenes (Fe-Px). Pyroxene crystallization histories can be interpreted as initial crystallization of pigeonite (low Ti/(Ti+Cr), Ti/Al = 1:4) followed by augite (Mg/(Mg + Fe) = $\geqslant$0.4, Ti/Al = 1:4 to 1:2) and finally Fe-rich pyroxene (high Ti/(Ti + Cr), Ti/Al = 1:2 to 1:1) such that in (B) the crystallization history of pyroxene runs counter clockwise from the Ti/Al intercept. The pyroxenes appear to record much of the crystallization history of major silicate and oxide phases in the LaPaz mare basalts (see text for details).

thickness (Grove and Walker, 1977) yield between 0.1–1 °C/h, during crystallization of plagioclase. This estimate is consistent with crystal size distribution studies of the LaPaz meteorites (Day et al., 2005b).

3.2.3. Olivine (3.3%)

Forsteritic olivine ($Fo_{40–67}$; Table 2; Fig. 6) occurs as sparsely scattered crystals that possess equant mineral habits and relatively large grain sizes ($\leqslant$0.8 mm), as well as extreme zonation from core to rim. Forsteritic olivines (Fo_{20} or greater) can possess resorbtion features and are overgrown by pigeonite. In some cases the forsteritic olivines adjoin mesostasis areas resulting in extreme Fe-enrichment (Fo_{64}–$Fo_{<5}$) at the rims of these crystals. Forsteritic olivines often contain chromite inclusions and, in at least

Table 3
Representative ion microprobe analyses of main silicate and accessory phases in LAP 02224 and LAP 02205

Sample:	LAP 02224												LAP 02205									
Phases:	Olivine (Fo_{64})		Olivine (Fo_{44})		Olivine (Fo_{31})		Px ($Wo_{22}En_{50}$)		Px ($Wo_{33}En_{34}$)		Px ($Wo_{25}En_{4}$)		Olivine (Fo_{62})		Px ($Wo_{35}En_{41}$)		Plagioclase		Apatite		Merrillite	
p.p.m		$\pm1\sigma$		$\pm1\sigma$		$\pm1\sigma$		$\pm1\sigma$		$\pm1\sigma$		$\pm1\sigma$		$\pm1\sigma$		$\pm1\sigma$		$\pm1\sigma$		$\pm1\sigma$		$\pm1\sigma$
Sc	12.7	0.1	11.6	0.2	10.3	0.1	115	1	138	1	51.3	0.4	12.0	0.2	118	1	3.70	0.28	—	—	—	—
V	80.7	0.3	53.4	0.5	17.5	0.2	453	2	484	2	5.9	0.2	62.7	0.6	388	3	2.65	0.14	—	—	—	—
Cr	3046	2	1799	4	606	1	8087	13	8571	14	183	1	2274	5	7564	22	5.55	0.21	—	—	—	—
Ni	799	4	481	7	236	3	536	10	602	10	358	6	—	—	—	—	—	—	—	—	—	—
Rb	0.77	0.09	0.59	0.13	0.71	0.12	0.26	0.43	0.85	0.47	0.48	0.37	1.56	0.26	0.13	0.44	0.07	2.35	—	—	—	—
Sr	0.37	0.02	0.29	0.02	0.11	0.01	6.03	0.25	8.23	0.28	4.37	0.16	1.25	0.07	6.00	0.32	214	2	—	—	—	—
Y	0.59	0.02	2.29	0.07	1.33	0.05	20.7	0.4	25.0	0.5	39.7	0.4	0.9	0.1	21.3	0.7	2.3	0.1	—	—	—	—
Zr	0.29	0.02	0.43	0.03	0.26	0.02	17.2	0.5	25.4	0.7	37.4	0.6	2.6	0.1	19.5	1.0	5.3	0.2	—	—	—	—
Ba	0.14	0.01	0.23	0.2	0.10	0.01	0.27	0.05	0.22	0.04	5.77	0.18	1.60	0.09	0.23	0.05	31.7	0.9	—	—	—	—
La	0.02	<0.01	0.23	0.02	0.03	0.01	0.41	0.05	0.48	0.05	1.27	0.08	<0.01	—	0.35	0.05	0.83	0.05	1225	14	4400	27
Ce	0.01	<0.01	0.44	0.02	0.03	0.01	4.11	0.24	6.07	0.35	3.96	0.19	<0.01	—	2.09	0.16	2.16	0.12	3723	28	11264	48
Pr	0.01	<0.01	0.05	<0.01	0.01	<0.01	0.37	0.04	0.53	0.05	0.79	0.05	<0.01	—	0.32	0.03	0.27	0.02	543	9	1396	14
Nd	0.02	<0.01	0.24	0.01	0.04	<0.01	2.59	0.13	3.44	0.17	1.20	0.15	<0.01	—	2.49	0.15	1.20	0.05	2695	27	6376	41
Sm	<0.01	<0.01	0.07	0.01	0.02	<0.01	1.13	0.11	1.68	0.14	2.04	0.13	<0.01	—	1.31	0.12	0.28	0.04	793	22	1782	33
Eu	<0.01	<0.01	<0.01	<0.01	<0.01	<0.01	0.07	0.01	0.11	0.01	0.12	0.02	<0.01	—	0.11	0.02	1.80	0.09	32.3	2.46	100	4
Gd	0.01	<0.01	0.13	0.02	0.05	0.01	2.26	0.16	3.41	0.20	3.21	0.26	<0.01	—	2.41	0.23	0.42	0.05	789	25	1836	37
Tb	<0.01	<0.01	0.04	<0.01	0.01	<0.01	0.49	0.04	0.63	0.06	0.65	0.06	0.02	<0.01	0.54	0.05	0.06	0.01	145	6	378	10
Dy	0.06	<0.01	0.27	0.01	0.13	0.01	3.82	0.18	4.21	0.22	5.78	0.21	0.11	0.01	3.88	0.22	0.43	0.03	856	16	2539	27
Ho	0.02	<0.01	0.06	0.01	0.04	<0.01	0.71	0.07	0.88	0.07	1.35	0.09	0.03	<0.01	0.72	0.10	0.12	0.01	173	6	547	11
Er	0.09	<0.01	0.24	0.01	0.17	0.01	2.38	0.12	2.67	0.16	4.83	0.17	0.30	0.01	3.08	0.18	0.30	0.03	383	11	1463	21
Tm	0.02	<0.01	0.05	0.01	0.3	<0.01	0.39	0.04	0.38	0.03	0.74	0.05	<0.01	—	0.34	0.04	<0.01	—	45.3	3.2	208	7
Yb	0.21	0.01	0.35	0.02	0.30	0.02	2.35	0.15	2.46	0.17	4.86	0.29	0.20	0.02	2.52	0.27	0.31	0.04	223	11	1208	23
Lu	0.04	<0.01	0.06	0.01	0.06	<0.01	0.33	0.04	0.38	0.05	0.97	0.07	0.04	0.01	0.34	0.07	0.05	0.01	24.6	3.5	147	8

Data for LAP 02205 from Anand et al. (2005).

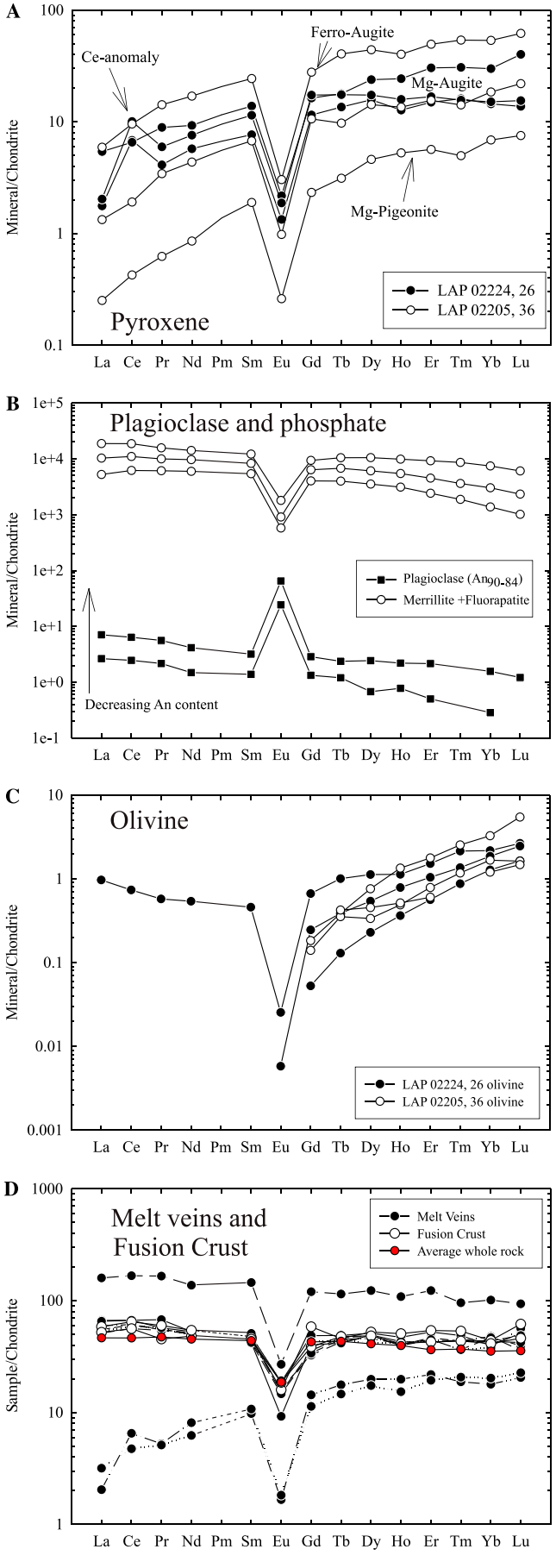

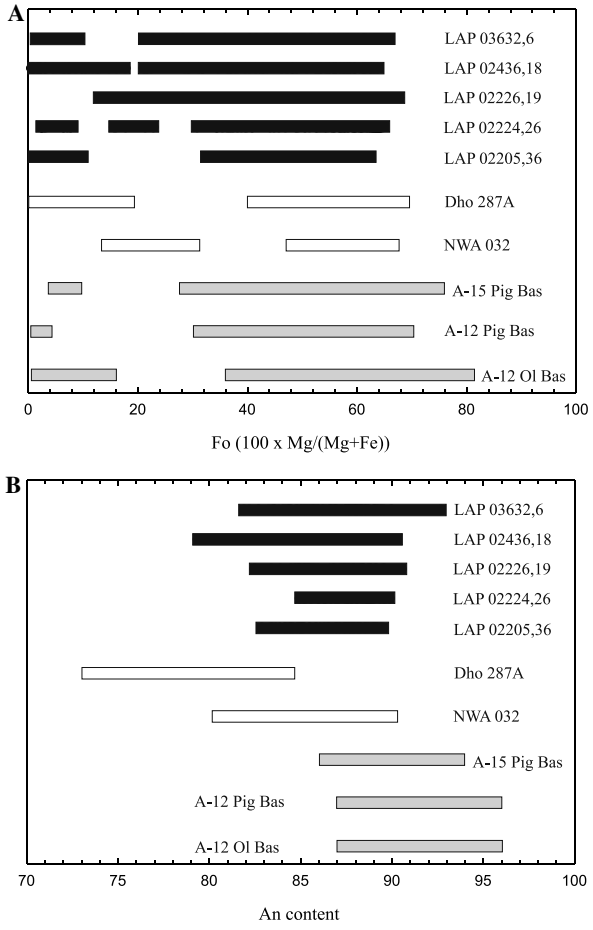

Fig. 6. Summary plots for the range of (A) forsterite and (B) anorthite compositions for LaPaz basalts, desert mare basalt meteorites Dhofar 287A and NWA032, A-15 and A-12 pigeonite normative basalts, and A-12 olivine basalts. Data from this study, Anand et al. (2003) and references therein.

one case (LAP 02226, 19), multiphase melt inclusions. The fayalitic olivines (Fo_{20} or less) are restricted to mesostasis areas where they occur with K–Ba-rich glass and silica. Olivine compositions are similar to the ranges seen in Apollo 12 and Apollo 15 basalts, as well as Dhofar 287A, but not to NWA 032 (Fig. 6). The meteorite NWA 032 lacks fayalitic olivines, consistent with the petrogenetic history of that basalt (Fagan et al., 2002). REE profiles of olivines

Fig. 5. CI-chondrite-normalized Rare Earth Element (REE) patterns for major and accessory mineral phases in LAP 02205 (from Anand et al., 2005) and LAP 02224. Pyroxenes (A) have broadly sub-parallel patterns; note the positive Ce-anomalies in some LAP 02224,26 pyroxenes, that are located close to the fusion crust of that meteorite. Plagioclase (B) have positive Eu anomalies, whilst phosphates contain a large proportion of the REE inventory of the LaPaz basalts. Olivines (C) in LAP 02224, 26 can exhibit LREE enrichment consistent with terrestrial alteration. Melt veins and fusion crusts (D) have broadly sub-parallel REE patterns to the whole rock, but melt veins can be variable due to their localized melting characteristics and the domination of mineralogies in those melt zones. Chondrite normalization values from Anders and Grevesse (1989).

Table 4
Representative EMPA data of major oxide phases and FeNi metals in LaPaz mare basalt meteorites

Phases:	Chromite					Ulvö spinel			Ilmenite		
Sample:	LAP 02205	LAP 02224	LAP 02226	LAP 02436	LAP 03632	LAP 02205	LAP 02436	LAP 02226	LAP 02436	LAP 03632	LAP 02226
wt%											
SiO_2	0.10	0.15	0.07	0.08	0.07	0.07	0.11	0.06	0.04	⩽0.03	⩽0.03
TiO_2	5.53	5.33	5.30	5.25	4.58	32.4	32.9	30.9	52.3	53.4	51.6
ZrO_2	—	—	⩽0.03	—	—	—	—	⩽0.03	—	—	⩽0.03
Al_2O_3	11.8	11.8	11.7	11.9	11.9	1.93	1.90	2.14	0.09	0.11	0.12
V_2O_3	0.83	0.77	0.75	0.77	0.74	0.20	0.20	0.31	—	—	—
Cr_2O_3	43.3	44.3	43.5	44.2	45.2	2.07	1.33	4.42	0.06	0.14	0.20
MgO	3.72	3.78	2.16	3.52	4.30	0.72	0.65	0.39	0.11	0.05	0.19
CaO	0.10	0.06	0.05	0.04	⩽0.03	0.12	0.09	0.09	⩽0.03	⩽0.03	0.08
MnO	0.26	0.19	0.30	0.21	0.21	0.31	0.30	0.30	0.37	0.29	0.38
FeO	32.9	32.1	35.0	33.1	31.4	61.2	61.8	60.3	46.4	46.3	46.6
Total	98.5	98.6	98.9	99.1	98.5	99.0	99.3	98.9	99.5	100.3	99.2
Cr#	65.4	66.1	65.9	66.0	67.1	5.8	3.8	11.9	—	—	—

Phases:	Troilite	FeNi metal									
Sample:	LAP 03632	LAP 02205	LAP 02205	LAP 02224	LAP 02224	LAP 02226	LAP 02226	LAP 02436	LAP 02436	LAP 03632	LAP 03632
wt%											
Fe	62.3	80.3	94.0	63.3	35.0	90.9	75.7	58.8	60.9	92.3	57.7
Co	0.09	3.42	1.37	5.51	2.45	1.73	3.60	3.64	6.00	1.39	5.20
Ni	0.07	15.8	5.46	29.4	59.8	7.52	1.5	37.1	31.5	5.41	35.2
Cr	⩽0.05	—	0.06	—	—	—	0.04	—	0.11	0.19	0.13
S	36.9	⩽0.05	⩽0.05	⩽0.05	0.07	⩽0.05	⩽0.05	⩽0.05	⩽0.05	⩽0.05	⩽0.05
P	0.14	0.05	⩽0.05	⩽0.05	⩽0.05	⩽0.05	⩽0.05	⩽0.05	⩽0.05	⩽0.05	⩽0.05
Si	0.10	0.12	⩽0.05	⩽0.05	⩽0.05	⩽0.05	⩽0.05	0.06	⩽0.05	⩽0.05	⩽0.05
Ti	0.11	—	—	—	—	—	—	—	—	0.21	0.14
Ca	0.22	—	—	—	—	—	—	—	—	0.10	0.11
Total	99.9	99.7	100.9	98.2	97.3	100.1	98.9	99.6	98.6	99.6	98.5

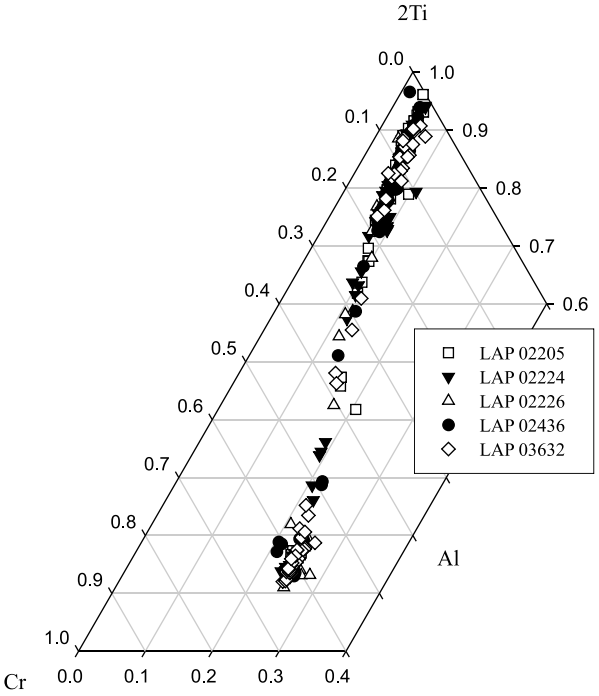

Fig. 7. Cr-Al-2Ti plot for spinels from the LaPaz basalts. A distinct compositional gap exists between the high-Al chromites and ulvöspinel. Results are similar to other mare basalts (e.g., Dhofar 287A, Apollo 12, Apollo 15; Anand et al., 2003 and references therein).

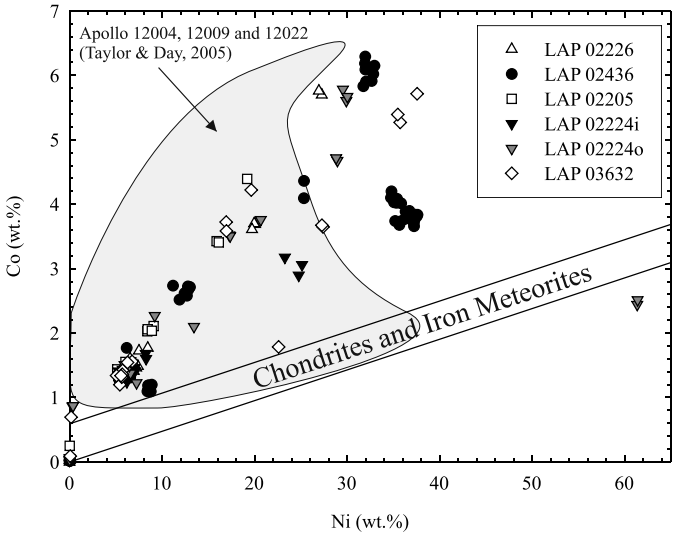

Fig. 8. Co vs. Ni contents (in weight percent) for the LaPaz basalts. Chondrite and iron meteorite data extrapolated from Goldstein and Yakowitz (1971) and Anders and Grevesse (1989). The LaPaz basalts possess similar FeNi metals to Apollo 12 mare basalts (Taylor and Day, 2005). These metals do not have an exogenous (i.e., meteoritic) origin.

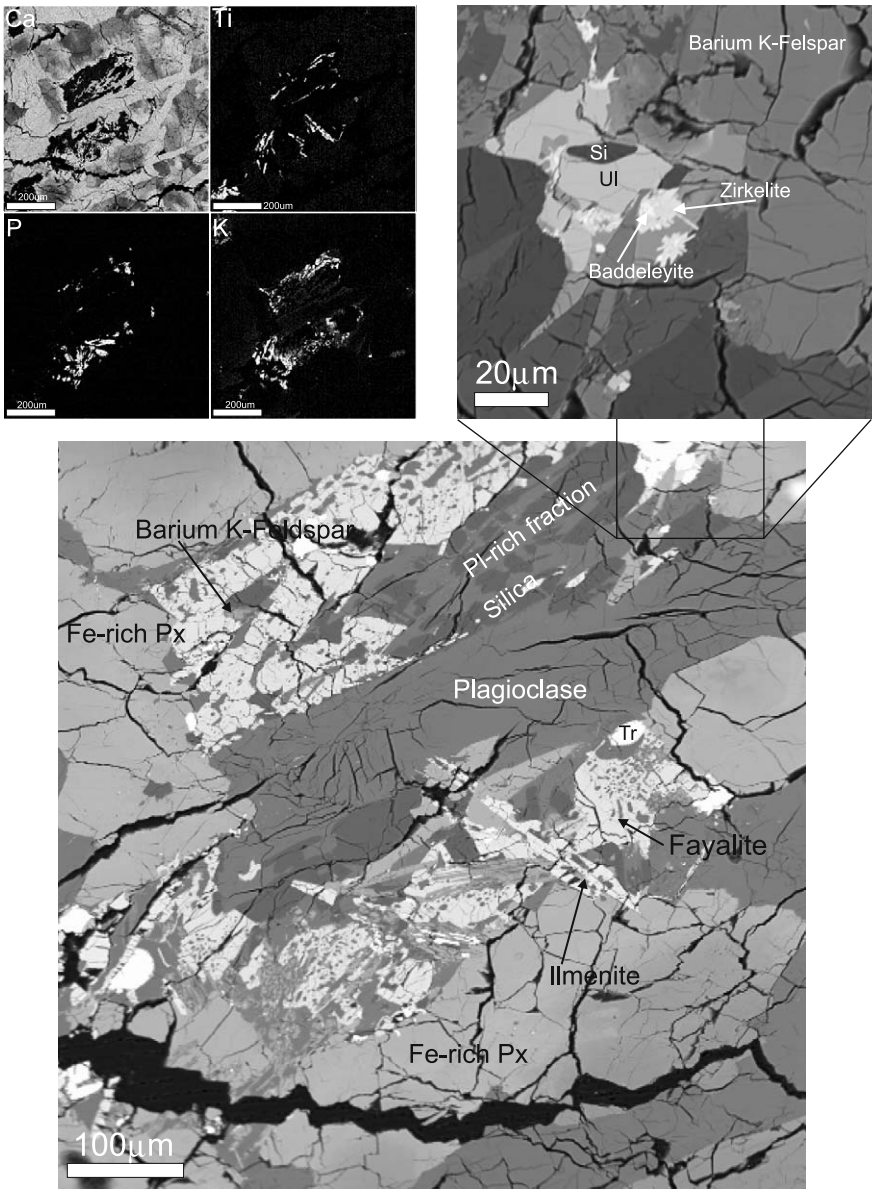

Fig. 9. Back-scattered electron (BSE) images and X-ray images of an area of mesostasis in LAP 03632. Main BSE image shows mesostasis pocket situated around an elongate plagioclase crystal and illustrates the 'swiss cheese' texture common to mare basalt mesostasis. Top right hand corner shows blow-up view of baddeleyite and zirkelite. Top left hand corner shows Ca, Ti, P, and K X-ray maps of the main image area illustrating the distribution of elements in the mesostasis.

from LAP 02224, 26 show increasing heavy REE (HREE) and light REE (LREE) enrichment towards the rims, where the Fo contents of the olivines, particularly adjoining mesostasis areas, are low (Fig. 5). The LREE enrichment seen in one olivine grain in Fig. 5 is probably the result of terrestrial weathering (e.g., Crozaz et al., 2003).

3.2.4. Opaques (4 %)

Ilmenite (average length and widths = 0.20×0.06 mm) is the most common opaque phase in the LaPaz basalts making up, on average, 3.4% of the polished sections. Ilmenite occurs as elongate grains, commonly with lamellar structures, indicative of shock (Taylor et al., 1971). Ilmenite compositions in all of the LaPaz basalts are nearly pure $FeTiO_3$, with the vast majority having no geikielite component ($MgTiO_3$) (<0.5 wt% MgO), although some samples possess ilmenites with MgO > 2 wt% (associated close to high Fo olivines), consistent with the large range in MgO for ilmenites in other lunar basalts (El Goresy, 1976). A small number of ilmenite grains contain significant MnO enrichments up to 0.4 wt% (Table 4).

Ulvöspinel (0.4%) and chromite (0.1%) are the second and third most abundant opaque minerals. Chromite formed during the earliest stages of the crystallization of the LaPaz basalts. Vanadium abundances are elevated in chromite but become increasingly depleted in ulvöspinel

Table 5
Representative EMPA and ion microprobe data of fusion crusts and melt veins for LaPaz mare basalt meteorites

	Melt vein	Fusion Crust	Melt veins					Fusion Crusts		
	LAP 02224	LAP 02224	LAP 02205	LAP 02224	LAP 02226	LAP 02436	LAP 03632	LAP 02224	LAP 02226	LAP 03632
no.			7	152	20	67	46	8	14	22
wt %										
SiO_2	43.1	43.4	46.2 (15)	43.5 (37)	42.3 (104)	44.9 (19)	46.4 (15)	43.6 (9)	42.7 (19)	43.3 (17)
TiO_2	2.96	3.01	1.43 (101)	3.08 (69)	2.20 (86)	2.66 (121)	1.59 (100)	3.34 (42)	3.33 (56)	3.71 (76)
Al_2O_3	11.4	11.52	19.7 (52)	11.3 (21)	12.0 (43)	14.4 (57)	17.5 (68)	9.1 (10)	7.29 (85)	8.3 (14)
Cr_2O_3	0.29	0.23	0.13 (4)	0.26 (8)	0.17 (14)	0.20 (13)	0.20 (23)	0.25 (5)	0.20 (10)	0.24 (19)
MgO	7.11	7.03	3.18 (60)	6.6 (16)	4.6 (25)	4.5 (20)	4.3 (34)	6.77 (115)	5.97 (59)	6.04 (206)
CaO	10.6	10.8	13.8 (18)	10.8 (11)	11.3 (31)	12.4 (14)	13.6 (15)	10.6 (2)	10.3 (10)	10.9 (9)
MnO	0.17	0.22	0.18 (5)	0.26 (6)	0.25 (10)	0.24 (9)	0.19 (10)	0.30 (8)	0.30 (7)	0.32 (2)
FeO	21.9	20.2	13.4 (68)	20.5 (26)	19.5 (66)	17.9 (55)	13.5 (53)	22.1 (16)	25.6 (25)	23.4 (24)
Na_2O	0.37	0.42	0.73 (20)	0.40 (9)	0.49 (18)	0.57 (23)	0.70 (33)	0.36 (4)	0.30 (7)	0.30 (7)
K_2O	0.11	0.14	0.15 (7)	0.13 (3)	0.12 (6)	0.12 (5)	0.13 (8)	0.12 (2)	0.17 (24)	0.13 (4)
P_2O_5	0.23	0.30	0.10 (3)	0.14 (9)	0.07 (5)	0.10 (7)	—	0.22 (5)	0.16 (9)	0.26 (9)
SO_2	1.04	0.34	0.45 (42)	0.34 (37)	0.51 (32)	0.32 (33)	—	0.08 (13)	0.30 (86)	0.05 (6)
Total	99.2	97.6	99.5	97.3	93.6	98.4	98.1	96.8	96.5	97.0
Mg#	36.7	38.3	29.7	36.4	29.4	30.9	36.2	35.3	29.4	31.5
p.p.m										
Sc	43.5 (8)	59.6 (7)								
V	83.0 (13)	87.2 (11)								
Cr	1913 (7)	1542 (6)								
Ni	501 (14)	427 (11)								
Rb	0.0 (13)	1.5 (13)								
Sr	129 (2)	125 (2)								
Y	76.8 (13)	88.6 (12)								
Zr	294 (4)	322 (3)								
Ba	119 (2)	110 (2)								
La	12.0 (6)	13.8 (6)								
Ce	33.9 (12)	39.1 (11)								
Pr	4.83 (37)	5.34 (32)								
Nd	22.7 (9)	24.6 (9)								
Sm	6.21 (58)	6.89 (56)								
Eu	0.82 (13)	0.89 (14)								
Gd	6.66 (96)	11.5 (9)								
Tb	1.64 (19)	1.67 (20)								
Dy	11.1 (6)	12.7 (6)								
Ho	2.28 (22)	2.82 (22)								
Er	7.12 (46)	8.60 (46)								
Tm	0.88 (9)	1.29 (12)								
Yb	7.59 (55)	7.16 (58)								
Lu	0.96 (14)	1.50 (16)								

Numbers in parentheses represent one SD of variance in terms of units cited.

with higher Ti contents, consistent with crystallization of ulvöspinel after pyroxene. Where chromite is in contact with the groundmass, it is surrounded by ulvöspinel, but this is not the case for chromites fully included within olivine or pyroxene. Spinel compositions in the LaPaz basalts follow a fractionation trend that is identical to those seen for the Apollo 12 and Apollo 15 mare basalts (Table 4: Fig. 7) (Taylor et al., 1971); analyses intermediate between chromite and ulvöspinel appear to be due to 'edge effects' because petrographic boundaries between the two are optically distinct.

Troilite occurs in the LaPaz basalts as poorly formed grains, normally at the edge of silicate and oxide crystals, or within the mesostasis (Table 4). LaPaz basalts contain FeNi metal grains with anomalously high Ni and Co abundances, unlike those found in typical achondrites, chondrites, or iron meteorites, but which are similar in composition to those present in some Apollo 12 basalts (Fig. 8). Ni and Co contents in LaPaz metals are positively correlated (Fig. 8; Taylor and Day, 2005), and range from <0.05–37.5 wt% and 0.1–6.3 wt%, respectively (Table 4). In the Apollo 12 mare basalts, FeNi metal grains are associated with earliest formed minerals (chromite, olivine) and are often located at the boundaries between the phenocrysts and matrix (Taylor and Day, 2005). Conversely, in the LaPaz basalts, the FeNi metal grains are sited within Fe-rich rims of pyroxene, or at the boundaries of ferropyroxene, plagioclase or ulvöspinel and, rarely, within troilite, indicating a late-stage formation. FeNi metal grains in both the Apollo 12 and LaPaz basalts

Table 6
Major and trace element compositions of LaPaz mare basalt meteorites

Sample:	LAP 02205	LAP 02224	LAP 02224	LAP 02226	LAP 02436	LAP 03632	Average	SD
Sub-ID:	21	17	18	13	20	8		
Position:	Centre	Outer	Centre	Centre	Centre	Centre		
n[a]:	15	15	15	15	15	15		
wt%								
SiO_2	46.0	45.9	45.3	45.3	45.3	45.7	*45.6*	*0.33*
TiO_2	3.11	2.94	3.27	3.20	3.23	3.26	*3.17*	*0.13*
Al_2O_3	9.95	9.45	9.95	10.07	9.52	9.65	*9.76*	*0.26*
Cr_2O_3	0.29	0.32	0.30	0.31	0.36	0.33	*0.32*	*0.03*
MgO	6.32	7.19	6.84	6.84	7.71	7.25	*7.02*	*0.47*
CaO	11.4	11.1	11.3	11.2	10.8	11.2	*11.2*	*0.20*
MnO	0.32	0.31	0.29	0.30	0.30	0.31	*0.31*	*0.01*
FeO[b]	21.8	22.1	22.0	22.0	22.1	21.7	*21.9*	*0.16*
Na_2O	0.39	0.35	0.38	0.35	0.33	0.33	*0.36*	*0.03*
K_2O	0.10	0.10	0.11	0.10	0.08	0.08	*0.10*	*0.01*
P_2O_5	0.17	0.17	0.16	0.16	0.13	0.12	*0.15*	*0.02*
SO_3	0.16	0.16	0.14	0.15	0.15	0.17	*0.15*	*0.01*
Total	100.0	100.0	100.0	100.0	100.0	100.0		
Mg#	34.1	36.8	35.6	35.7	38.4	37.3		

ppm							BHVO-1[c] Durham	SD	Certified
Sc	52.8	59.2	57.3	58.8	54.0	58.4	33.9	2.5	31.8
V	92	114	109	110	110	113	320	3	317
Cr	1625	2368	2172	2192	2298	2300	297	4	289
Co	35.4	37.6	36.9	36.9	37.5	37.9	46.8	0.8	45.0
Ni	42.4	20.6	18.5	21.9	26.0	21.8	142	2	121
Cu	18.6	19.8	19.4	18.6	16.4	19.8	143	2	136
Zn	27.5	30.8	29.6	27.1	26.3	30.2	115	3	84
Ga	3.74	4.29	4.07	4.18	3.58	4.28	21.2	0.3	21.0
Rb	1.67	1.86	1.74	1.82	1.50	1.79	9.41	0.06	11
Sr	109	124	122	122	104	124	404	2	403
Y	57.0	64.9	64.9	64.0	55.1	64.5	27.4	0.1	27.6
Zr	172	194	190	185	161	189	174	1	179
Nb	11.9	13.3	12.9	12.8	11.1	13.2	19.6	0.8	19.0
Cs	0.03	0.04	0.04	0.04	0.02	0.02	0.12	0.04	0.13
Ba	122	137	131	134	112	134	131	2	139
La	9.97	11.4	11.5	11.5	10.2	11.5	15.2	0.2	15.8
Ce	26.3	29.6	29.3	30.6	25.3	29.8	36.2	0.4	39.0
Pr	4.04	4.57	4.5	4.67	3.93	4.61	5.53	0.07	5.7
Nd	19.1	21.5	21.5	21.9	18.6	21.6	25.1	0.3	25.2
Sm	6.05	6.75	6.73	6.79	5.84	6.87	6.10	0.04	6.2
Eu	0.98	1.10	1.07	1.11	0.93	1.13	2.03	0.03	2.1
Gd	7.81	9.08	8.73	8.92	7.57	9.04	6.31	0.05	6.4
Tb	1.44	1.64	1.62	1.65	1.41	1.64	0.95	0.01	0.96
Dy	9.35	10.6	10.4	10.6	9.1	10.6	5.17	0.08	5.2
Ho	2.00	2.30	2.21	2.28	1.94	2.28	0.97	0.01	0.99
Er	5.40	6.09	6.04	6.08	5.26	6.10	2.34	0.05	2.4
Tm	0.84	0.95	0.94	0.95	0.82	0.96	0.33	0.01	0.33
Yb	5.30	5.95	5.91	5.92	5.12	5.97	1.98	0.03	2.02
Lu	0.82	0.93	0.90	0.91	0.79	0.92	0.30	0.01	0.29
Hf	4.50	5.02	4.92	4.90	4.25	5.00	4.33	0.05	4.38
Ta	0.60	0.68	0.65	0.65	0.57	0.67	1.23	0.03	1.23
Pb	0.71	0.84	0.80	0.82	0.68	0.81	2.11	0.09	2.6
Th	1.79	2.04	2.04	2.06	1.72	2.03	1.25	0.03	1.08
U	0.45	0.49	0.50	0.50	0.43	0.49	0.41	0.01	0.42

[a] Number of analyses of fused beads for major element analysis, average and SD calculated from all analyses.
[b] FeO represents total Fe.
[c] BHVO-1 replicate analyses during ICP-MS analysis of LaPaz basalts. Certified values from Ottley et al. (2003) and references therein.

show no systematic relationships between Co and Ni contents and location within their respective oxide and silicate host minerals.

3.2.5. Mesostasis (~3%)

The mesostasis possesses a 'swiss-cheese' texture, due to the highly fractionated nature of the LaPaz basalts and the

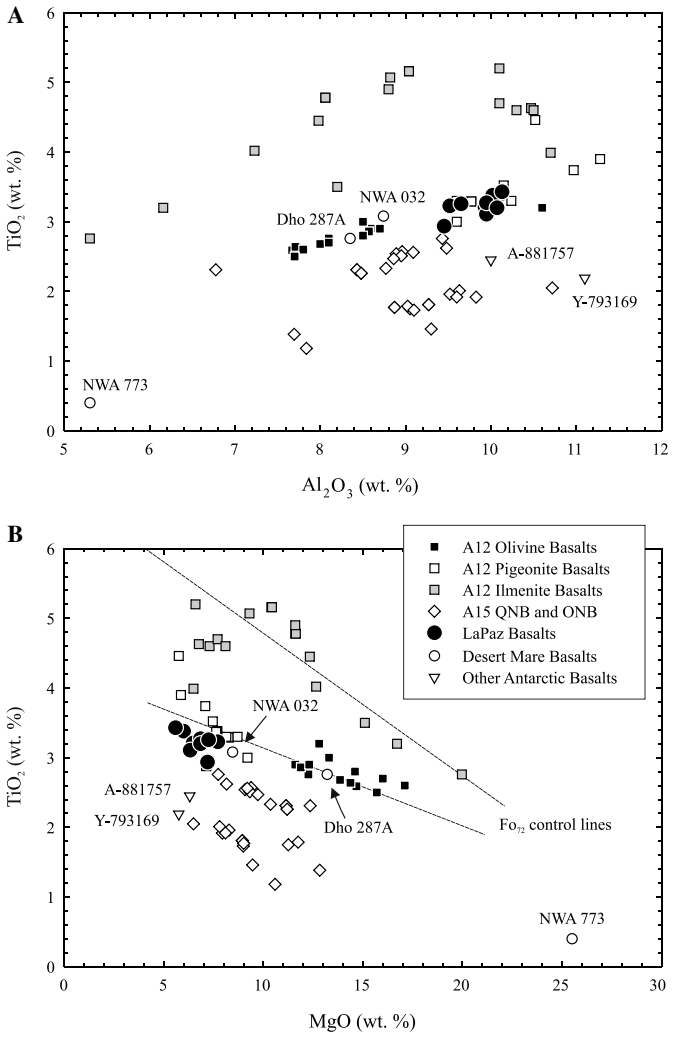

Fig. 10. Plot of whole rock TiO_2 (in weight percent) versus (A) Al_2O_3 and (B) MgO for LaPaz basalts (data from this study). For comparison data for low-Ti mare basalts are also shown (from Rhodes and Hubbard, 1973; Rhodes et al., 1977; Neal et al., 1994) along with mare basalt meteorite data (Warren and Kallemeyn, 1989, 1993; Fagan et al., 2002, 2003; Anand et al., 2003). Forsterite control lines are from Rhodes et al. (1977). Note the similarities of LaPaz basalts to both Apollo 12 pigeonite basalts and to NWA 032.

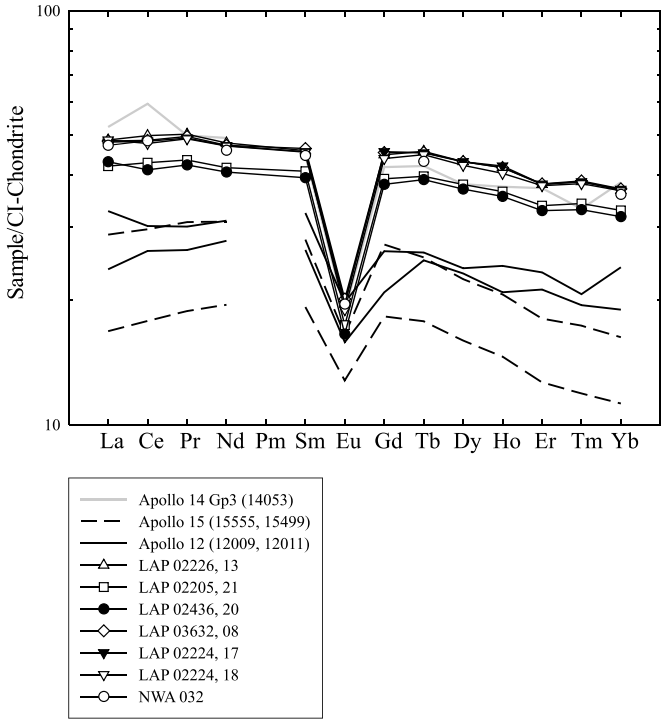

Fig. 11. CI-chondrite-normalized REE patterns for LaPaz whole rocks compared with Apollo 12 and Apollo 15 data (from Snyder et al., 1997; Neal, 2001). LaPaz basalts have similar REE patterns to NWA 032 and to Apollo 14 Group 3 basalts (after Dickinson et al., 1985). Variations in absolute abundance in the LaPaz data are probably the result of 'nuggeting' of REE-rich phases in the prepared sample powders. This variation does not affect the trace element ratios which are essentially invariant among the LaPaz basalts. Chondrite normalization values from Anders and Grevesse (1989).

effect of silicate-liquid immiscibility that occurs after ~95% crystallization of a lunar basaltic magma (e.g., Taylor et al., 1971; Rutherford et al., 1974; Hess et al., 1978; Neal and Taylor, 1989, 1991). These areas of mesostasis are identical to those described by Anand et al. (2003) for Dhofar 287A. The mesostasis is composed predominantly of a symplectic intergrowth of fayalite and potassium-rich glass with minor silica (cristobalite/tridymite; Table 2). Fluorapatite, rare merrillite, as well as ilmenite, FeNi metal, barium K-feldspar, baddeleyite, and zirkelite (cuspate morphology) also occur in the mesostasis (Tables 2 and 4; Fig. 9). The fluorapatites contain between 0.7 and 3.2 wt% F, less than 1 wt% Cl and up to 1 wt% Ce_2O_3 and La_2O_3, whereas the merrillite contains up to 4 wt% Ce_2O_3. These phosphates contain a large proportion of the incompatible element and REE budget of the LaPaz basalts. High REE contents measured by EMPA are supported by elevated incompatible and REE concentrations of merrillite (>5.6 wt%) and fluorapatite (>1.9 wt%) measured by ion microprobe (Fig. 5). Estimation of the total REE content from ion microprobe measurements would sum the total oxide weight percents of merrillite measured by EMPA to ~100% (Tables 2 and 3).

3.2.6. Fusion crust and shock-induced melt veins (1.7%)

Fusion crust covers 50–95% of the LaPaz meteorite exteriors and has been preserved on three of the polished mounts (LAP 02224, 26, LAP 02226, 19, and LAP 03632, 21) forming a veneer around the sample in the range of 50–100 μm thick (Fig. 2). The fusion crust is vesiculated, much like that around lunar regolith breccia meteorites (e.g., Fig. 2). The compositions of the fusion crust around the LaPaz basalts are similar to each other and to the compositions of the melt veins and whole rock compositions (Table 5; Fig. 5). REE patterns for the fusion crust are flat with pronounced negative Eu anomalies, similar to whole rock trace element abundances (Fig. 5).

Sinuous, brown colored, zoned melt veins occur in the LaPaz basalts forming a dendritic melt vein network (Fig. 2). Lack of cross-cutting relations between melt veins

suggests formation from a singular shock event, possibly during the launching event for the LaPaz meteorites. 3-D spatial constraints are currently unavailable for the melt veins because of destruction of this information during the allocation process (C. Satterwhite, personal communication) meaning reconstruction of the melt vein network in the basalts is difficult. The melt veins range up to 200 μm in thickness and are indicative of intense, instantaneous shock of the basalt host. These veins have the same general trace element abundances as the fusion crust (Table 5). The melt veins also contain small iron-rich phases and zones of compositional variation due to localized melting of olivine, pyroxene or fluorapatite, resulting in heterogeneous major and trace element abundances and pronounced LREE depletion or enrichment relative to their HREE contents (Fig. 5). Compared to the fusion crusts, the melt veins have a larger range of Cr (1200–2100 ppm) concentrations, but generally possess flat REE patterns with pronounced negative Eu-anomalies (Fig. 5).

3.3. Bulk rock major and trace element geochemistry

Bulk major and trace element data for the LaPaz basalts are presented in Table 6. LaPaz basalts possess relatively low MgO contents compared with other low-Ti lunar basalts. Mg-numbers range from 34 to 38 for the LaPaz basalts, similar to the range seen in previously discovered Antarctic mare basalt meteorites (Mg-number = 33–37; Y-793169, A-881757 and EET 87521; Warren and Kallemeyn, 1989, 1993) and to some Apollo 12 pigeonite- and ilmenite-bearing and Apollo 15 quartz-normative basalts. Using the mare basalt classification scheme of Neal and Taylor (1992), the LaPaz basalts are classed as low-Ti, low-Al, low-K basalts (Fig. 10). In this respect, they are similar to Apollo 15 quartz-normative basalts but are most similar to Apollo 12 pigeonite basalts (Fig. 10). LaPaz basalts, along with NWA 032 and Dhofar 287A, lie on the trend of Apollo 12 pigeonite and olivine basalts defined by Neal et al. (1994) and do not appear to correlate with other ferroan mare basalt meteorites (e.g., Y-793169 and A-881757; Fig. 10).

For a given Mg-number, the LaPaz basalts are more enriched in incompatible trace elements than Apollo 12, 15 and other Antarctic lunar basalts, but have similar incompatible element abundances to desert meteorite NWA 032. For example, the LaPaz basalts have $(La/Yb)_n = 1.31 \pm 0.03$, $Rb/Sr = 0.0147 \pm 0.0004$, $Sm/Nd = 0.314 \pm 0.003$ and $U/Th = 0.244 \pm 0.004$ ($n = 6$). Compared with Apollo 12 ($(La/Yb)_n = 0.76$–1.55, $Rb/Sr = 0.005$–0.021, $Sm/Nd = 0.30$–0.38 and $U/Th = 0.23$–0.49) and Apollo 15 samples ($(La/Yb)_n = 1.49$–2.08, $Rb/Sr = 0.007$–0.010, $Sm/Nd = 0.25$–0.37 and $U/Th = 0.24$–0.35), the incompatible element and REE ratios of the LaPaz mare basalts are most similar to Apollo 12 mare basalts. Relative to the mare basalt meteorites, the LaPaz basalts have $(La/Yb)_n$ ratios that are lower than NWA 032 (2.27; Fagan et al., 2002) and higher than Y-793169, A-881757 and predominantly basaltic breccia EET 87521/96008 (0.79–0.98; Warren and Kallemeyn, 1989, 1993).

LaPaz basalts have higher chondrite-normalized REE abundances than the majority of low-Ti basalts from the Apollo and Luna sample collections, with the notable exception of some small Apollo 14 (Group 3) aluminous basalt fragments (Dickinson et al., 1985) (Fig. 11). Of the other mare basalt meteorites, only NWA 032 has REE abundances and patterns similar to that of the LaPaz mare basalts, consistent with the similar Th/Sm ratios of those samples (LaPaz = 0.300 ± 0.004; NWA 032 = 0.29). LaPaz basalts have strong negative Eu anomalies, with $Eu/Eu^* (Eu_n/\sqrt{(Sm_n \times Gd_n)}) = 0.431 \pm 0.006$, and variable trace element abundances. This variability in REE abundances probably reflects the small aliquot sizes prepared and 'nuggeting' of incompatible-elements into inhomogeneously distributed phosphates or REE-rich minerals, similar to effects seen on a smaller scale within melt veins. Relative to Apollo 12 and 15 basalts, the LaPaz basalts are LREE-enriched, a feature that cannot easily be ascribed to the effects of terrestrial weathering (Crozaz et al., 2003). We note that the interior and exterior portions of LAP 02-224 possess trace element abundances within error of one another and show no significant variations in trace element ratios normally susceptible to weathering, such as Ce/Nb. Therefore, the LREE-enriched nature of the LaPaz basalts is a primary petrogenetic signature that sets them apart from all mare basalts with the notable exception of NWA 032 and some aluminous Apollo 14 basalts.

4. Discussion

4.1. Lunar origin and pairing of the LaPaz mare basalts

Pyroxenes ($Fe/Mn = 64 \pm 13$, 1 SD, $n = 818$) and olivines ($Fe/Mn = 96 \pm 12$, 1 SD, $n = 902$) in the LaPaz basalts possess lower Mn for a given Fe content, than pyroxene ($Fe/Mn = \sim 45$) and olivine ($Fe/Mn = \sim 75$) in typical unfractionated terrestrial basalts. This distinct mineral chemical signature is considered characteristic of a lunar origin (Fe/Mn in pyroxene = ~79 and in olivine ~105; Papike et al., 2003) because Mn/Fe ratios appear to be unique indicators of planetary bodies (Drake et al., 1989). In addition, the LaPaz mare basalts also possess FeNi metals, as well as $\Delta^{17}O$ that is indistinguishable from the terrestrial-lunar mass fractionation line (Spicuzza, M.J., et al., unpublished data). The relatively unaltered nature and ancient age relative to terrestrial basalts (~2.9 Ga; Anand et al., 2005; Nyquist et al., 2005) for the LaPaz meteorites, along with their unique chemistry (FeNi metals, anhydrous nature, low fO_2) and oxygen isotope compositions firmly place their origin as lunar mare basalts.

Meteorites LAP 02205, LAP 02224, LAP 02226, LAP 02436, and LAP 03632 are almost certainly paired. This pairing is probably related to break-up in Earth's atmosphere considering the close spatial arrangement of the meteorites in the LaPaz Icefield, where many meteorites

have been concentrated by sublimation processes acting on the host ice. Apart from possessing nearly identical mineral modes, mineral and whole rock major and trace element compositions, the LaPaz mare basalt meteorites also share additional common features such as the presence of shock-induced melt veins, anomalous FeNi metal and nearly identical textures (e.g., Fig. 1; Day et al., 2005b). The confirmed pairing of these meteorites means that they represent a significant mass of low-Ti, evolved mare basalts with which to compare with Apollo mare basalts and volcanic glasses and upon which to perform detailed geochemical studies (e.g., Day et al., 2005a; Taylor and Day, 2005).

4.2. Post-crystallization effects on chemistry: weathering, fusion, shock-induced melting

The LaPaz basalts possess both fusion crusts and a network of brown melt veins. Studying compositions of fusion crusts and melt veins is important for two reasons:

(1) It provides quantitative evidence whether they record whole rock compositions of the meteorites. Preservation of this information would allow relatively non-destructive techniques (e.g., EMPA, Ion Microprobe) to be used on small meteorite finds and would enhance confidence in interpretation of these chemical signatures. For assessment, we compare analyses of melt veins and fusion crust with large homogenized whole rock samples.
(2) It is important to know whether the melt veins in the LaPaz meteorites possess exogenous meteoritic (i.e., non lunar) material. Ultimately, understanding if fusion crusts and melt veins disturb the initial emplacement chemical signatures of meteorite precursor lithologies is of great importance prior to interpreting petrogenetic events on the meteorites' host planet.

LaPaz fusion crust compositions (Table 5) are marginally more FeO-rich and MgO-poor than the whole rock and possess more elevated TiO_2 such that on a ternary plot of Al_2O_3–TiO_2–MgO (Fig. 12) the field of fusion crust compositions is displaced from whole rock compositions. Trace element abundances and REE patterns are similar for the fusion crust and the whole rock (Table 5, Fig. 5). Higher abundances of Ti and Ni and lower abundances of Cr in the fusion crust probably relate to inefficient melting of chromian-spinel and efficient melting of olivine and ilmenite during friction-induced melting with Earth's atmosphere. There is also evidence for disturbance of low abundance (sub-ng/g level) highly siderophile elements (HSE), either during fusion or via terrestrial alteration through preservation in the Antarctic ice (Day et al., 2005a). Alteration at exposed surfaces of the LaPaz meteorites is similarly demonstrated by Ce-anomalies in some pyroxenes and LREE enrichments in some olivines from LAP 02224 (Fig. 5). It is important to note, however, that

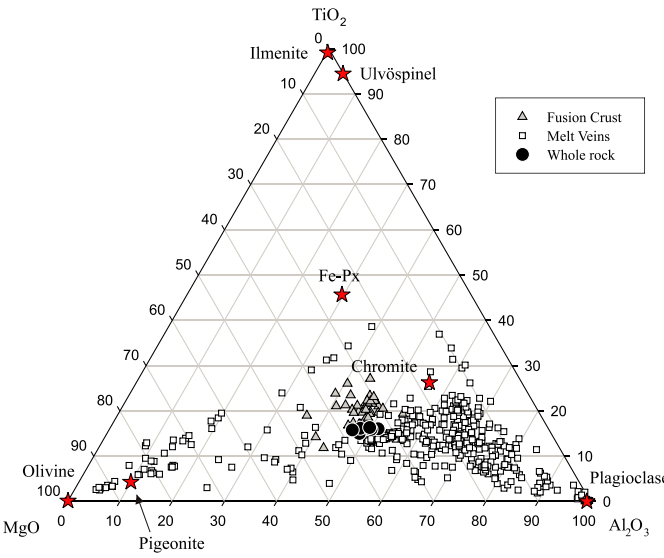

Fig. 12. Ternary plot of MgO–TiO_2–Al_2O_3 for LaPaz whole rock samples, melt vein and fusion crust analyses. Also shown are end-member mineral compositions for LaPaz basalts. Large variations in the composition of the LaPaz melt veins reflect the localized melting of minerals in the basalts immediately due to an impact-induced shock event.

the LaPaz basalts are relatively free from terrestrial alteration.

Melt veins exhibit a range in major and trace element compositions (Table 5, Fig. 5). In Fig. 12, melt veins exhibit a broad array of compositions with the vast majority being Al_2O_3-enriched relative to whole rock and fusion crust compositions. Chemical heterogeneity directly relates to size and location of melt veins. For example, small (<50 μm) melt veins and outermost linings of large melt veins (>50 μm) exhibit ranges in major and trace element compositions relating to minerals that they abut. Conversely, large melt veins are typically zoned with an inhomogeneous outer layer and a homogenized centre (e.g., Fig. 2). This variation is similarly demonstrated in the REE patterns of the melt veins (Fig. 5), where low REE abundances relate to melting of silicate phases, whereas high REE abundances occur on addition of REE-rich phosphates; only the centers of large melt veins have REE patterns similar to that of the fusion crust. In summary, although the LaPaz melt veins and fusion crusts retain the overall geochemical compositions of the basalts, they may not faithfully record the initial isotopic or elemental compositions of their host meteorite.

Shock-induced melt veins within the LaPaz basalts possess no exogenous material. These melt veins formed from a single event and apparently represent localized melting of the basalt itself. Melt veins with an exogenous origin (i.e., implanted into the host basalt) would be expected to possess relatively homogeneous major and trace element compositions that are different from the host basalt. The low (⩽ppt-level) HSE contents and supra-chondritic $^{187}Os/^{188}Os$ also provide evidence for the endogenous origin of melt veins (and metals) in the LaPaz basalts (Day et al., 2005a). This is because even a minor (<0.001%) con-

tribution from HSE-rich chondrite or iron meteorite material would dominate the low HSE abundances and $^{187}Os/^{188}Os$ isotope compositions of these basalts.

4.3. Crystallization processes

4.3.1. Eruption conditions

It is well established that Apollo mare basalts were erupted with high eruption temperatures, low oxygen fugacities and correspondingly high FeO contents relative to terrestrial basaltic volcanism (e.g., Warren, 2003). It has also been recognized that the large variety of textures in the Apollo mare basalts, including porphyritic and vitrophyric textures, can mostly be explained by relatively simple cooling histories (e.g., Lofgren et al., 1975; Grove and Walker, 1977). The LaPaz basalts, despite their evolved bulk compositions relative to Apollo 12 and 15 basalts, were erupted at relatively high temperatures and low oxygen activities and have experienced a relatively simple cooling history (Day et al., 2005b). The average calculated eruption temperature for the LaPaz basalts, using two independent methods (Roeder, 1974 and using a $K_D = 0.32 \pm 0.03$; Jones, 2003), is 1183 ± 6 °C. Relative oxygen fugacity is typical of mare basalts at $fO_2 =$ 0–2 log units below the IW buffer using the method of Papike et al. (2004), which indicates $V^{3+} > V^{4+}$ for LaPaz basalts ($V \times 100/(Cr + Al) = 1.36 \pm 0.09$ (atomic), cut off Cr-number = 60). Quantitative petrological constraints, eruption conditions, and eruption temperature, appear to be similar to those of the less-evolved Apollo 12 and 15 low-Ti basalts (~1150–1350 °C; Papike et al., 1998).

4.3.2. Origin of FeNi metal grains in mare basalts?

One of the most striking features of the LaPaz basalts is that they possess FeNi metal grains with anomalously high Ni and Co abundances similar to those discovered in Apollo 12 basalts (Reid et al., 1970; Brett et al., 1971; Taylor and Day, 2005). FeNi metal grains in Apollo 12 basalts have previously been considered as the result of reduction of the melt through fractional crystallization of silicate and oxide phases which had elevated partition coefficients for Co and Ni (Reid et al., 1970; Brett et al., 1971). The process of reduction, although potentially valid for the Apollo 12 basalts, does not seem an appropriate explanation for LaPaz FeNi metal grains. Expectation would be for the high Co and Ni metal grains to be hosted in early formed minerals, with low Co and Ni metal grains formed later in the fractionation sequence; this is not observed. The possibility that Ni and Co became relatively incompatible during crystallization of late-stage pyroxene and plagioclase appears unlikely considering high Ni contents measured in pyroxenes (e.g., Table 3). A meteoritic (i.e., exogenous origin) can also be ruled out based on the trends of Co and Ni in the LaPaz basalts (Fig. 8) and the lack of evidence for meteoritic contamination from Re-Os isotope systematics (Day et al., 2005a). Alternative explanations might include reaction or assimilation of olivine and pyroxene releasing Ni and Co into the melt, or the reduction of Ni and Co through low oxygen activities. There is evidence for olivine resorbtion in the LaPaz basalts; however, the overall observations made here suggest re-evaluation may be required for the origin of high Co and Ni metal grains in mare basalts.

4.4. Parental liquids for the LaPaz mare basalts

LaPaz basalts underwent significant fractional crystallization during petrogenesis and are unlikely to reflect primary magmatic liquids. For example, they have elevated incompatible-element abundances relative to their Mg-number and have olivine and pyroxene mineral trends that show extreme Fe-enrichment (Figs. 3 and 6). Low-Ti, low-Al, low-K compositions suggest the most suitable analogues for LaPaz parental magmas come from less fractionated Apollo 12 and Apollo 15 basalts or from low-Ti volcanic glasses because fractionation will act to decrease Mg/Fe and increase TiO_2 and incompatible trace elements. Prior to assessing parental magma compositions of LaPaz basalts, confirmation is required that they represent original melt compositions and are not an amalgamation of cognate and non-cognate material. The first line of evidence to suggest minerals are cognate comes from the lack of mixed crystal populations (Day et al., 2005b). The second line of evidence comes from REE compositions of individual minerals. Estimated equilibrium melt REE patterns, of the bulk rock from REE abundances in minerals can be compared with whole rock REE patterns and their agreement is a strong indication of closed-system crystallization.

REE compositions of melts in equilibrium with the earliest formed minerals are identical to that of the measured whole rock REE compositions of the LaPaz basalts (Anand et al., 2005). Equilibrium crystallization of the LAP 02205 whole rock composition using the MELTS program yielded a near identical crystallization sequence and mineral compositions to that observed, but predicted lower forsterite contents for olivine than actually measured in the LaPaz basalts (Anand et al., 2005). Whole rock Mg-numbers (34–38) for the LaPaz basalts presented here are in equilibrium with the olivine cores (Fo_{58-64}) defining a K_D of 0.32 ± 0.03; this confirms that the LaPaz basalts reflect an original melt composition based upon previously determined K_D for lunar glasses and basalts (Delano, 1980). Therefore, the overall bulk compositions of the LaPaz mare basalts reflect an original melt composition and indicate closed-system fractional crystallization after emplacement.

A prerequisite for the parental magma of the LaPaz mare basalts is that it was a low-Ti, low-Al, low-K precursor much like olivine-phyric low-Ti Apollo 12 and Apollo 15 basalts or pyroclastic glasses recovered during Apollo missions. Simple lever-rule addition of 20-25% olivine ($Fo_{73.4}$; e.g., Brett et al., 1971) and chromite (Cr-number = >65) (relative accumulation ratios of olivine:chromite of 95:5) to the LaPaz basalts would result in relative decrease in whole rock FeO (20–21 wt%), have limited impact on SiO_2 (44–45 wt%) and Al_2O_3 (8–9 wt%) and sub-

stantially increase MgO (11–15 wt%) and Cr_2O_3 (0.7–1.0 wt%). These calculations indicate that the implied primary melt for the LaPaz basalts is similar to some Apollo 12 and Apollo 15 basalts that are thought to represent liquid compositions (e.g., 12004, 12006, and 15672) or to some low-Ti yellow or green glasses (Delano, 1986). Mineral accumulation and removal processes are clearly significant in lunar basalt petrogenesis. For example, the olivine-gabbro clast present in NWA 773 possesses 25.5 wt% MgO and is related to accumulation of olivine at shallow levels (Jolliff et al., 2003). The very low TiO_2 content of such a clast might also be reasonably attributed to reflect the lack of accumulation of phases rich in titanium (e.g., ilmenite, ulvöspinel). The LaPaz basalts could reflect the residua after accumulation of olivine and chromite to form a cumulate lithology such as NWA 773.

4.5. Assimilation versus source signature for incompatible element enrichment?

From a major element perspective the LaPaz basalts appear to be similar to low-Ti Apollo 12 pigeonite basalts and could be a fractionation product of more primitive low-Ti mare basalts or pyroclastic glasses. This would imply that the LaPaz basalts represent fractionated melts from a magmatic system that was fed by similar degrees of partial melting of a mantle source like that of Apollo low-Ti mare basalts or pyroclastic glasses. However, LaPaz mare basalts (~2.9 Ga; Anand et al., 2005; Nyquist et al., 2005) cannot be directly related to these low-Ti basalts or pyroclastic glasses because Apollo low-Ti mafic rocks are significantly older (~3.1–3.7 Ga; Snyder et al., 2000) and have lower incompatible element abundances for their relative Mg-number. The presence of incompatible element enrichments in lunar materials is commonly taken to be indicative of a KREEP component (K, REE, P, U, Th, etc.) and the LaPaz basalts do possess a KREEP-like REE pattern (Fig. 11). The KREEP signature is an important feature of lunar petrogenesis whose formation has been considered using a variety of models of variable complexity (e.g., Shih, 1977; Hess et al., 1978; Neal and Taylor, 1989; Warren, 2003). A general axiom among lunar investigators is that a KREEP reservoir (often referred to as ur-KREEP), representing enrichment of incompatible elements as the melt residua of a lunar magma ocean, formed early in lunar history (~4.36 ± 0.06 Ga, e.g., Lugmair and Carlson, 1978).

In the LaPaz basalts, elevated incompatible element signatures are dominated by the late-stage mesostasis minerals. These minerals represent the concentration of incompatible elements during closed-system, in situ fractional crystallization and are simply a scaled version of incompatible element enrichment in a lunar magma ocean (e.g., Neal and Taylor, 1991). An outstanding question regarding incompatible element enriched signatures such as those found in the LaPaz basalts is when this KREEP component was added to the magma. Assimilation and fractional crystallization (AFC) models have previously been advocated for enrichment of incompatible elements in some Apollo mare basalt suites (e.g., Dickinson et al., 1985). In these models KREEP material was assimilated by mafic melts derived from the mantle as they rose to the lunar surface. In an alternative model, Borg et al. (2004, 2005) suggested incompatible enrichment in olivine gabbro clast NWA 773 (2.87 ± 0.03 Ga) represented a mantle source component. This model, especially for younger mare basalts, is appealing because (1) it would account for the melting of material over a prolonged period of time in the lunar mantle due to the concentration of heat-producing radionuclides (i.e., U and Th), and (2) it would also explain the correlation between incompatible element enrichment in the source region and age (Fig. 2 of Borg et al., 2004).

Modeling of AFC or bulk mixing is not entirely satisfactory considering the clustering of the LaPaz data. However, if the models are considered realistic, incompatible element enrichment in the LaPaz basalts can be approximated by ~5% bulk mixing but by >20% AFC of a KREEP-rich component (Fig. 13). Such large amounts of AFC seem untenable and bulk mixing also seems unlikely considering that it would require two distinct melts to generate these mixing trends. As noted by Borg et al. (2004), KREEP assimilation models appear inconsistent with the correlation of incompatible element abundances and age. Additionally, considering similarities in major element compositions, it is unclear how older low-Ti Apollo 12 and 15 mare basalts apparently assimilated less of a KREEP component than young (~2.8–3.0 Ga) LaPaz basalts, NWA 032 or NWA 773. The only plausible explanation for such differences might be that a KREEP-like component is unevenly distributed in the lunar crust or mantle and that these meteorites come from source regions totally disparate from the Apollo mare basalt samples. It is also unclear what the physical constraints on assimilation of a KREEP component are and how assimilation might affect major element compositions of lunar magmas.

Despite these caveats, a key limitation on when a KREEP-like component was added to LaPaz magmas comes from the trace element patterns of pyroxenes within the LaPaz basalts. Because pyroxenes formed throughout most of the crystallization history of the LaPaz basalts they should track any addition of assimilated material. Although there are increases in LREE/HREE and incompatible element ratios, they are entirely consistent with increasing fractionation and vary in a relatively systematic manner (e.g., La/Yb = 0.14–0.26 in pyroxene). The overall REE patterns of the pyroxenes are sub-parallel and liquids in equilibrium with the earliest formed pyroxenes are identical to whole-rock compositions (Anand et al., 2005). These results are consistent with closed-system crystallization of the LaPaz mare basalts (Fig. 5). Therefore incompatible enrichment to the LaPaz mare basalts is unlikely to have occurred during crystallization placing further constraints on the likelihood of AFC processes.

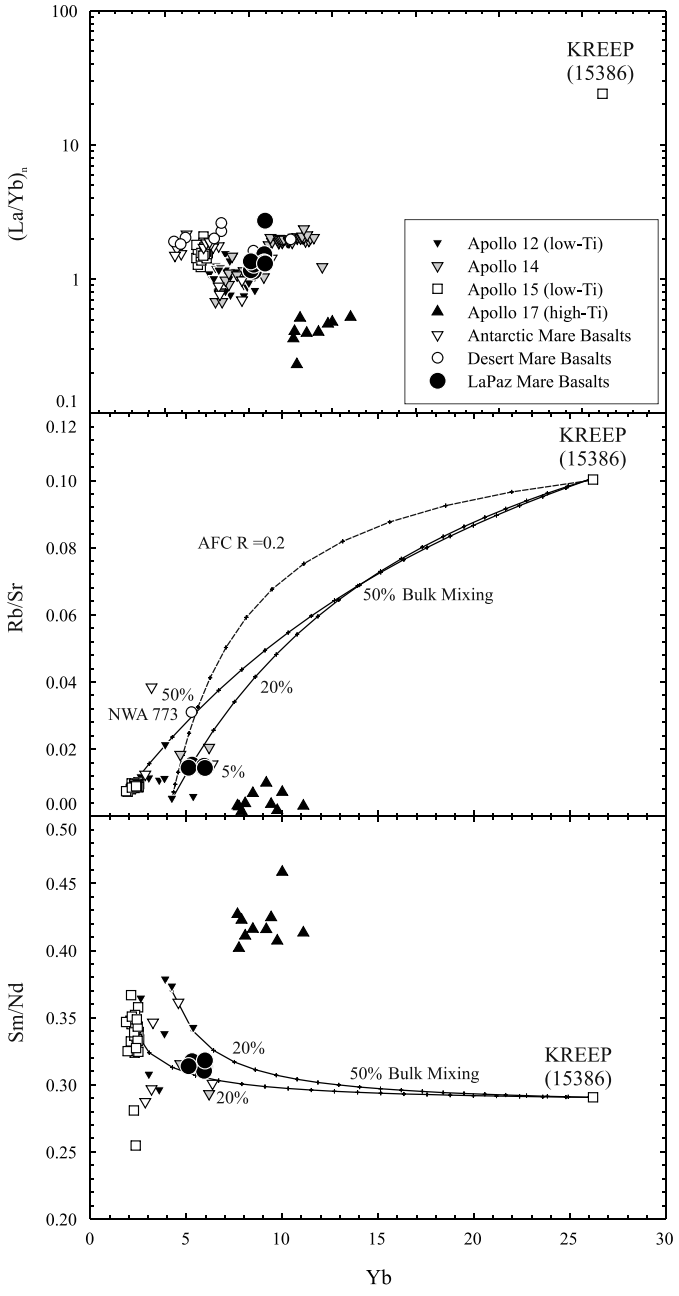

Fig. 13. Plots of Yb versus $(La/Yb)_n$ (normalized to chondrite), Rb/Sr and Sm/Nd for LaPaz mare basalts. Also shown are data for Apollo 12, 14, 15, and 17 rocks and published Antarctic and desert mare basalts. Simple bulk mixing trajectories are constructed between KREEP-rich rock 15386 (Yb = 26 ppm, Rb/Sr = 0.1, Sr = 187 ppm, Sm/Nd = 0.29, and Nd = 126 ppm), A12 basalt (Yb = 4.3 ppm, Rb/Sr = 0.005, Sr = 75 ppm, Sm/Nd = 0.37, and Nd = 11 ppm) and A15 basalt (Yb = 1.9 ppm, Rb/Sr = 0.007, Sr = 96 ppm, Sm/Nd = 0.35, and Nd = 8.4 ppm). Also shown is an assimilation and fractional crystallization (AFC) curve with $R = 0.2$ and bulk D = 1. Crosses on the modeled curves are increments of 5%. LaPaz basalts cluster, but indicate that unfeasibly large amounts of AFC are required to explain the incompatible element enriched signature of these basalts. Mixing models for NWA 773 have resulted in a similar conclusion (Borg et al., 2005). Published data is from Dickinson et al. (1985), Neal (2001), Fagan et al. (2002, 2003), Anand et al. (2003), Neal and Kramer (2003) and references therein.

4.6. Source regions on the moon and implications for KREEP

The age and chemical composition of the LaPaz basalts is similar to some previously discovered meteorites. Ziegler et al. (2005) have suggested that the LaPaz basalts may be related to NWA 032 based on their ages and gross geochemical compositions. From a compositional perspective such pairing is entirely possible, with only minor addition or subtraction of chromite, olivine and pigeonite required to explain the chemical variability between NWA 032 and LaPaz basalts. Texturally, NWA 032 and the LaPaz basalts are different. LaPaz has had a relatively simple crystallization history of continuous nucleation and growth (Day et al., 2005b), whereas NWA 032 records a two-stage cooling history indicating order of magnitude differences in cooling rate (Fagan et al., 2002). These textural constraints do not impede possible pairing because variations in texture may simply reflect different fractional crystallization and cooling histories for products of the same magmatic system. Olivine gabbro NWA 773, a cumulate rock, also has a similar age and KREEP-like signature to the LaPaz basalts and NWA 032 but the large differences in chemical compositions and texture make any attempts at trying to geochemically link these meteorites difficult.

A number of general observations may be made regarding the unbrecciated mare basalt meteorites found on Earth to date (Y-793169; A-881757; NWA 032; NWA 773; Dhofar 287A; LaPaz):

(1) All are low-Ti to VLT basalts and appear to originate by similar degrees of partial melting from a mantle source region similar to those responsible for the Apollo 12 and 15 low-Ti basalts.
(2) Mare basalt meteorites represent lavas or near surface magma bodies similar to Apollo basalts.
(3) The majority of the mare basalt meteorites found possess low Mg-numbers (LaPaz = 34–38—this study; Y-793169 = 32.6, A-881757 = 33.3—Warren and Kallemeyn, 1993; NWA 032 = 39—Fagan et al., 2002) apart from NWA 773 (68.9—Fagan et al., 2003) and Dhofar 287A (51.6—Anand et al., 2003), indicative of strong fractionation of these melt products.
(4) So far, the dated, unbrecciated mare basalt meteorites fall within two age ranges; from ~2.8 to ~3.0 Ga for the LaPaz basalts, NWA 032 and the NWA 773 olivine gabbro clast (Fagan et al., 2002; Borg et al., 2004; Anand et al., 2005), and ~3.8 to 3.9 Ga for A-881757 and Y-793169 (Misawa et al., 1993; Torigoye-Kita et al., 1995).
(5) The younger suite (2.9 Ga) of mare basalts and Dhofar 287A possess elevated incompatible element concentrations and relatively high Rb/Sr and La/Yb ratios relative to older low-Ti mare basalts.

Combined, these first-order observations suggest a close temporal and geochemical linkage between some of the mare basalt meteorites. Lunar Prospector gamma-ray Th and FeO (Lawrence et al., 2000) and Clementine spectral reflectance TiO_2 data (Lucey et al., 2000) place constraints on likely source regions for the LaPaz and other mare basalt meteorites. For LaPaz (and NWA 032) orbital remote sensing constraints offer a number of provenances including some portions of the Procellarum KREEP Terrane and Mare Humorum, Mare Fecundatis, western Mare Serenatatis and Mare Crisium.

5. Conclusions

Results of a comprehensive mineral and whole rock major and trace element study are presented for five paired lunar meteorites from the LaPaz Icefield, Antarctica that have identical mineralogies, textures and geochemical compositions. The important conclusions regarding the petrogenesis of the LaPaz basalts are that:

1. They represent a liquid which crystallized as a closed system resulting in extreme fractionation manifested as Fe-enrichment and silicate-liquid immiscibility and the formation of mesostasis. This mesostasis contains the bulk of the incompatible element inventory of these basalts.
2. They contain FeNi metals with unusually high Co and Ni contents, similar to some Apollo 12 basalts but which are distinct from other chondritic and achondritic FeNi metals.
3. The crystallization conditions and evolved nature of the LaPaz basalts are consistent with fractionation of olivine and chromite from a parental liquid similar in composition to some olivine-phyric Apollo 12 and Apollo 15 basalts or lunar low-Ti pyroclastic glasses.
4. Young reported ages for LaPaz mare basalts (~2.9 Ga) and relative incompatible element enrichment compared to Apollo mare basalts and pyroclastic glasses indicates they cannot be directly related to one another. Instead LaPaz mare basalts may represent fractionated melts from a magmatic system that was fed by similar degrees of partial melting of a mantle source like that of the Apollo mare basalts or pyroclastic glasses, but which possessed greater incompatible element enrichment.
5. Despite textural differences, the LaPaz basalts and mare basalt meteorite NWA 032 have similar ages and compositions and may originate from a similar region on the Moon.

Acknowledgments

We thank C.J. Ottley for assistance with trace element analysis. The exceptionally constructive comments and suggestions of B.L. Jolliff, M.D. Norman, and Associate Editor C. Koeberl improved the quality of this work. This research has been supported through NASA Grants NAG 5-10414, NAG 5-11558, and NNG04GG49G.

Associate editor: Christian Koeberl

References

Alexander, C.M.O.D., 1994. Trace element distributions within ordinary chondrite chondrules: implications for chondrule formation conditions and precursors. *Geochim. Cosmochim. Acta* **58**, 3451–3467.

Anand, M., Taylor, L.A., Misra, K.C., Demidova, S.I., Nazarov, M.A., 2003. KREEPy lunar meteorite Dhofar 287A: a new lunar mare basalt. *Meteor. Planet. Sci.* **38**, 485–499.

Anand, M., Taylor, L.A., Floss, C., Neal, C.R., Terada, K., Tanigawa, S., 2005. Petrology and geochemistry of LAP 02205: a new low-Ti mare basalt meteorite. *Geochim. Cosmochim. Acta*, in press, doi:10.1016/j.gca.2005.08.018.

Anders, E., Grevesse, N., 1989. Abundances of the elements: meteoritic and solar. *Geochim. Cosmochim. Acta* **53**, 197–214.

Bence, A.E., Papike, J.J., 1972. Pyroxenes as recorders of lunar basalt petrogenesis: chemical trends due to crystal–liquid interaction. *Proc. Lunar Sci. Conf. 3rd.*, 431–469.

Borg, L.E., Shearer, C.K., Asmerom, Y., Papike, J.J., 2004. Prolonged KREEP magmatism on the Moon indicated by the youngest dated lunar igneous rock. *Nature* **432**, 209–211.

Borg, L.E., Shearer, C.K., Asmerom, Y., Papike, J.J., 2005. Geochemical and isotopic systematics of the youngest dated lunar igneous rock, Northwest Africa 773. Lunar Planet. Sci. XXXVI, CD-ROM#1026 (abs).

Brett, R., Butler Jr., P., Meyer Jr., C., Reid, A.M., Takeda, H., Williams, R., 1971. Apollo 12 igneous rocks 12004, 12008, 12009 and 12022: a mineralogical and petrological study. *Proc. Lunar Sci. Conf. 2nd*, 301–317.

Crozaz, G., Floss, C., Wadhwa, M., 2003. Chemical alteration and REE mobilization in meteorites from hot and cold deserts. *Geochim. Cosmochim. Acta* **67**, 4727–4741.

Day, J.M.D., Pearson, D.G., Taylor, L.A., 2005a. ^{187}Re–^{187}Os isotope disturbance of the La Paz mare basalt meteorites. *Lunar Planet. Sci.* XXXVI, CD-ROM #1424 (abs.).

Day, J.M.D., Taylor, L.A., Hill, E., Liu, Y., 2005b. Textural analysis of the La Paz mare basalt meteorites. *Meteor. Planet. Sci.* **40**, A37 (abs).

Delano, J.W., 1980. Chemistry and liquidus phase relations of Apollo 15 red glass: implications of the deep lunar interior. *Proc. Lunar Planet. Sci. Conf. 11th*, 251–288.

Delano, J.W., 1986. Pristine lunar glasses: criteria, Data, and Implications. *J. Geophys. Res.* **91**, D201–D213.

Dickinson, T., Taylor, G.J., Keil, K., Schmitt, R.A., Hughes, S.S., Smith, M.R., 1985. Apollo 14 aluminous mare basalts and their possible relationship to KREEP. *J. Geophys. Res.* **90**, C365–C374.

Drake, M.J., Newsom, H.E., Capobianco, C.J., 1989. V, Cr and Mn in the earth, moon, EPB, and SPB and the origin of the moon: experimental studies. *Geochim. Cosmochim. Acta* **53**, 2101–2111.

El Goresy, A., 1976. Oxide minerals in lunar rocks. In: Rumble, D., IIIIII (Ed.), *Oxide Minerals*, vol. 3. Mineralogical Society of America, Reviews in Mineralogy, pp. EG1–EG46.

Fagan, T.J., Taylor, G.J., Keil, K., Bunch, T.E., Wittke, J.H., Korotev, R.L., Joliff, B.L., Gillis, J.J., Haskin, L.A., Jarosewich, E., Clayton, R.N., Mayeda, T.K., Fernandez, V.A., Burgess, R., Turner, G., Eugster, O., Lorenzetti, S., 2002. Northwest Africa 032: product of lunar volcanism. *Meteor. Planet. Sci.* **37**, 371–394.

Fagan, T.J., Taylor, G.J., Keil, K., Hicks, T.L., Killgore, M., Bunch, T.E., Wittke, J.H., Mittlefehldt, D.W., Clayton, R.N., Mayeda, T.K., Eugster, O., Lorenzetti, S., Norman, M.D., 2003. Northwest Africa 773: lunar origin and iron-enrichment trend. *Meteor. Planet. Sci.* **38**, 529–554.

Floss, C., Crozaz, G., 1991. Ce anomalies in the LEW85300 eucrite: evidence for REE mobilization during Antarctic weathering. *Earth Planet. Sci. Lett.* **107**, 13–24.

Floss, C., James, O.B., McGee, J.J., Crozaz, G., 1998. Lunar ferroan anorthosite petrogenesis: clues from trace element distributions in FAN subgroups. *Geochim. Cosmochim. Acta* **62**, 1255–1283.

Goldstein, J.I., Yakowitz, H., 1971. Metallic inclusions and metal particles in the Apollo 12 lunar soil. *Proc. Lunar. Sci. Conf. 2nd*, 177–191.

Gnos, E., Hofmann, B.A., Al-Kathiri, A., Lorenzetti, S., Eugster, O., Whitehouse, M.J., Villa, I.M., Jull, A.J.T., Elkenberg, J., Spettel, B., Krähenbühl, U., Franchi, I.A., Greenwood, R.C., 2004. Pinpointing the source of a lunar meteorite: implications for the evolution of the Moon. *Science* **305**, 657–659.

Grove, T.L., Walker, D., 1977. Cooling histories of Apollo 5 quartz-normative basalts. *Proc. Lunar. Sci. Conf. 8th*, 1501–1520.

Hess, P.C., Rutherford, M.J., Campbell, H.W., 1978. Ilmenite crystallization in non-mare basalt: genesis of KREEP and high Ti-mare basalt. *Proc. Lunar. Planet. Sci. Conf. 9th*, 705–724.

Hsu, W., 1995. Ion microprobe studies of the petrogenesis of enstatite chondrites and eucrites. Ph.D. Thesis. Washington University.

Jolliff, B.L., Korotev, R.L., Zeigler, R.A., Floss, C., 2003. Northwest Africa 773: lunar mare breccia with a shallow-formed olivine-cumulate component, inferred very-low-Ti (VLT) heritage and a KREEP connection. *Geochim. Cosmochim. Acta* **67**, 4857–4879.

Jones, J.H., 2003. A liquidus geothermometer for SNC. *Lunar and Eucritic magmas. Lunar Planet. Sci.*, XXXIV, CD-ROM #1130 (abs.).

Kieffer, S.W., Schaal, R.B., Gibbons, R.V., Hörz, F., Milton, D.J., Dube, A., 1976. Shocked basalt from Lonar Impact Crater, India, and experimental analogs. *Proc. Lunar. Sci. Conf. 2nd*, 1391–1412.

Korotev, R.L., 2004. A unique chunk of the Moon. *Science* **305**, 622–623.

Lawrence, D.H., Feldman, W.C., Barraclough, B.L., Binder, A.B., Elphic, R.C., Maurice, S., Miller, M.S., Prettyman, T.H., 2000. Thorium abundances on the lunar surface. *J. Geophys. Res.* **105**, 20307–20331.

Lofgren, G.E., Donaldson, C.H., Usselman, T.M., 1975. Geology, petrology, and crystallization of Apollo 15 quartz-normative basalts. *Proc. Lunar. Sci. Conf. 6th*, 79–99.

Lucey, P.G., Blewett, D.T., Jolliff, B.L., 2000. Lunar iron and titanium abundance algorithms based on final processing of Clementine ultraviolet-visible images. *J. Geophys. Res.* **105**, 20297–20305.

Lugmair, G.W., Carlson, R.W., 1978. The Sm-Nd history of KREEP. *Proc. Lunar Planet. Sci. Conf. 9th*, 689–704.

McBride, K., McCoy, T., Welzenbach, L., 2004. LAP 02224, 02226 and 02436. In: Satterwhite, C., Righter, K. (Eds.), *Antarctic Meteorite Newsletter*, vol. 26, No. 2. Available from: <http://www-curator.jsc.nasa.gov/curator/antmet/amn/amn.htm>.

Misawa, K., Tatsumoto, M., Dalrymple, G.B., Yanai, K., 1993. An extremely low U/Pb source in the moon—U–Th–Pb, Sm–Nd, Rb–Sr, and Ar-40/Ar-39 isotopic systematics and age of lunar meteorite Asuka 881757. *Geochim. Cosmochim. Acta* **57**, 4687–4702.

Neal, C.R., 2001. Interior of the Moon: the presence of garnet in the primitive deep lunar mantle. *J. Geophys. Res.* **106**, 27865–27885.

Neal, C.R., Taylor, L.A., 1989. Metasomatic products of the lunar magma ocean: the role of KREEP dissemination. *Geochim. Cosmochim. Acta* **53**, 529–541.

Neal, C.R., Taylor, L.A., 1991. Evidence for metasomatism of the lunar highlands and the origin of whitlockite. *Geochim. Cosmochim. Acta* **55**, 2965–2980.

Neal, C.R., Taylor, L.A., 1992. Petrogenesis of mare basalts: a record of lunar volcanism. *Geochim. Cosmochim. Acta* **56**, 2177–2211.

Neal, C.R., Kramer, G., 2003. The composition of KREEP: a detailed study of KREEP basalt 15386. *Lunar Planet. Sci.*, XXXIV, CD-ROM #2023 (abs.).

Neal, C.R., Hacker, M.D., Snyder, G.A., Taylor, L.A., Liu, Y.-G., Schmitt, R.A., 1994. Basalt generation at the Apollo 12 site, Part 1: new data, classification and re-evaluation. *Meteoritics* **29**, 334–348.

Nyquist, L.E., Shih, C.-Y., Reese, Y., Bogard, D.D., 2005. Age of lunar meteorite LAP 02205 and implications for impact-sampling of planetary surfaces. *Lunar Planet. Sci.*, XXXIV, CD-ROM #1374 [abs.].

Ottley, C.J., Pearson, D.G., Irvine, G.I., 2003. A routine method for the dissolution of geological samples for the analysis of REE and trace elements via ICP-MS. In: Holland, J.G., Tanner, S.D. (Eds.), *Plasma Source Mass Spectrometry Applications and Emerging Technologies*. Royal Society of Chemistry Special Publication, pp. 221–230.

Papike, J.J., Ryder, G., Shearer, C.K., 1998. Lunar Samples. In: Papike, J.J. (Ed.), *Planetary Materials*, vol. 36. Reviews in Mineralogy, pp. 5.1–5.234.

Papike, J.J., Karner, J.M., Shearer, C.K., 2003. Determination of planetary basalt parentage: A simple technique using the electron microprobe. *Am. Min.* **88**, 469–473.

Papike, J.J., Karner, J.M., Shearer, C.K., 2004. Comparative planetary mineralogy: V/(Cr + Al) systematics in chromite as an indicator of relative oxygen fugacity. *Am. Min.* **89**, 1557–1560.

Reid, A.M., Meyer, C., Harmon, R.S., Brett, R., 1970. Metal grains in Apollo 12 igneous rocks. *Earth Planet. Sci. Lett.* **9**, 1–5.

Rhodes, J.M., Hubbard, N.J., 1973. Chemistry, classification and petrogenesis of Apollo 15 mare basalts. *Proc. Lunar Sci. Conf. 4th*, 1127–1148.

Rhodes, J.M., Blanchard, D.P., Dungan, M.A., Brannon, J.C., Rodgers, K.V., 1977. Chemistry of Apollo 12 mare basalts: Magma types and fractionation processes. *Proc. Lunar Sci. Conf. 8th*, 1305–1338.

Roeder, P.L., 1974. Activity of iron and olivine solubility in basaltic liquids. *Earth .Planet. Sci. Lett.* **23**, 397–410.

Rutherford, M.J., Hess, P.C., Daniel, G.H., 1974. Experimental liquid line of decent and liquid immiscibility for basalt 70017. *Proc. Lunar. Sci. Conf. 5th*, 569–583.

Shih, C.-Y., 1977. Origin of KREEP basalts. *Proc. Lunar Sci. Conf. 8th*, 2375–2401.

Snyder, G.A., Neal, C.R., Taylor, L.A., Halliday, A.N., 1997. Anatexis of lunar cumulate mantle in time and space: clues from trace-element, strontium and neodymium isotopic chemistry of parental Apollo 12 basalts. *Geochim. Cosmochim. Acta* **61**, 2731–2747.

Snyder, G.A., Borg, L.E., Nyquist, L.E., Taylor, L.A., 2000. Chronology and isotopic constraints on lunar evolution. In: Canup, R.M., Righter, K. (Eds.), *Origin of the Earth and Moon*. University of Arizona Press, Tuscon, pp. 361–395.

Taylor, L.A., Day, J.M.D., 2005. FeNi metal grains in La Paz mare basalt meteorites and Apollo 12 basalts. *Lunar Planet. Sci.*, XXXVI, CD-ROM #1417 [abs.].

Taylor, L.A., Kullerud, G., Bryan, W.B., 1971. Opaque mineralogy and textural features of Apollo 12 samples and a comparison with Apollo 11 rocks. *Proc. Lunar. Planet. Sci. Conf. 2nd*, 855–871.

Taylor, L.A., Patchen, A., Taylor, D.H.S., Chambers, J.G., McKay, D.S., 1996. X-ray digital imaging petrography of lunar mare soils: Modal analysis of minerals and glasses. *Icarus* **124**, 500–512.

Torigoye-Kita, N., Misawa, K., Dalrymple, G.B., Tatsumoto, M., 1995. Further evidence for a low U/Pb source in the moon: U-Th-Pb, Sm-Nd and Ar-Ar isotope systematics of lunar meteorite Yamato-793169. *Geochim. Cosmochim. Acta* **59**, 2621–2632.

Warren, P.H., 2003. The Moon. In: Davis, A.M. (Ed.), *Treatise in Geochemistry*, vol. 1, 559–599.

Warren, P.H., Kallemeyn, G.W., 1989. Elephant Moraine 87521: The first lunar meteorite composed of predominantly mare material. *Geochim. Cosmochim. Acta* **53**, 3323–3330.

Warren, P.H., Kallemeyn, G.W., 1993. Geochemical investigation of two lunar mare meteorites: Yamato-793169 and Asuka-881757. *Proc. NIPR Symp. Antarct. Meteor.* **6**, 35–57.

Ziegler, R.A., Korotev, R.L., Jolliff, B.L., Haskin, L.A., 2005. Petrography and geochemistry of the LaPaz ice field basaltic lunar meteorite and source-crater pairing with Northwest Africa 032. *Meteor. Planet. Sci.* **40**, 1073–1102.

Zinner, E., Crozaz, G., 1986a. A method for the quantitative measurement of rare earth elements by ion microprobe. *Int. J. Mass Spec. Ion Proc.* **69**, 17–38.

Zinner, E., Crozaz, G., 1986b. Ion probe determination of the abundances of all the rare earth elements in single mineral grains. In: Benninghoven, A., Colton, R.J., Simons, D.S., Werner, H.W. (Eds.), *Secondary Ion Mass Spectrometry, SIMS V*. Springer, New York, pp. 444–446.